



Chromosome-Scale Genome Assemblies of Aphids Reveal Extensively Rearranged Autosomes and Long-Term Conservation of the X Chromosome

Thomas C. Mathers ^{*,1} Roland H.M. Wouters,¹ Sam T. Mugford,¹ David Swarbreck,² Cock van Oosterhout,^{*,3} and Saskia A. Hogenhout ^{*,1}

¹Department of Crop Genetics, John Innes Centre, Norwich Research Park, Norwich, United Kingdom

²Earlham Institute, Norwich Research Park, Norwich, United Kingdom

³School of Environmental Sciences, University of East Anglia, Norwich, United Kingdom

*Corresponding authors: E-mails: thomas.mathers@jic.ac.uk; c.van-oosterhout@uea.ac.uk; saskia.hogenhout@jic.ac.uk

Associate editor: Ouangraoua Aida

Abstract

Chromosome rearrangements are arguably the most dramatic type of mutations, often leading to rapid evolution and speciation. However, chromosome dynamics have only been studied at the sequence level in a small number of model systems. In insects, Diptera and Lepidoptera have conserved genome structure at the scale of whole chromosomes or chromosome arms. Whether this reflects the diversity of insect genome evolution is questionable given that many species exhibit rapid karyotype evolution. Here, we investigate chromosome evolution in aphids—an important group of hemipteran plant pests—using newly generated chromosome-scale genome assemblies of the green peach aphid (*Myzus persicae*) and the pea aphid (*Acyrtosiphon pisum*), and a previously published assembly of the corn-leaf aphid (*Rhopalosiphum maidis*). We find that aphid autosomes have undergone dramatic reorganization over the last 30 My, to the extent that chromosome homology cannot be determined between aphids from the tribes Macrosiphini (*Myzus persicae* and *Acyrtosiphon pisum*) and Aphidini (*Rhopalosiphum maidis*). In contrast, gene content of the aphid sex (X) chromosome remained unchanged despite rapid sequence evolution, low gene expression, and high transposable element load. To test whether rapid evolution of genome structure is a hallmark of Hemiptera, we compared our aphid assemblies with chromosome-scale assemblies of two blood-feeding Hemiptera (*Rhodnius prolixus* and *Triatoma rubrofasciata*). Despite being more diverged, the blood-feeding hemipterans have conserved synteny. The exceptional rate of structural evolution of aphid autosomes renders them an important emerging model system for studying the role of large-scale genome rearrangements in evolution.

Key words: Hemiptera, *Myzus persicae*, *Acyrtosiphon pisum*, insect genome assembly, synteny, sex chromosome, karyotype evolution.

Introduction

Mutation generates genomic novelty upon which natural selection and genetic drift can act to drive evolutionary change (Charlesworth 2009; Lynch et al. 2016; Charlesworth and Charlesworth 2017; Good et al. 2017). Primarily, sequence-level studies of genome evolution have focused on single-nucleotide polymorphisms and small indels. However, with the advent of long-read sequencing and other technologies that capture long-range linkage information, we are now able to study the effects of larger mutational events such as segmental duplications, deletions, and other complex structural variants (e.g., Chakraborty et al. 2018; Kronenberg et al. 2018). Chromosomes may undergo extensive rearrangement via inversions, translocations, fusions, and fissions (Eichler and Sankoff 2003). These macromutations can have dramatic

consequences by altering gene regulation (Farré et al. 2019; Stewart and Rogers 2019) and modifying local recombination rates (Farré et al. 2013; Martin et al. 2019), and they are implicated in key evolutionary processes such as adaptation and speciation (Rieseberg 2001; Kirkpatrick and Barton 2006; Chang et al. 2013; Guerrero and Kirkpatrick 2014; Fuller et al. 2019; Wellband et al. 2019). Chromosome-scale genome sequencing and assembly are required to study such macromutations, and recent advances in genome assembly have reinvigorated the field (e.g., Dudchenko et al. 2017; Bracewell et al. 2019, 2020; Schield et al. 2019; Tandonnet et al. 2019; Teterina et al. 2020). So far, in insects, these studies have been restricted to a few holometabolous groups, such as Diptera (mainly *Drosophila* and mosquitoes) and Lepidoptera (butterflies) that have been the focus of concerted genome sequencing efforts.

© The Author(s) 2020. Published by Oxford University Press on behalf of the Society for Molecular Biology and Evolution.

This is an Open Access article distributed under the terms of the Creative Commons Attribution License (<http://creativecommons.org/licenses/by/4.0/>), which permits unrestricted reuse, distribution, and reproduction in any medium, provided the original work is properly cited.

Open Access

Comparative genomics of Diptera and Lepidoptera has revealed conservation of whole chromosomes or chromosome arms (i.e., macrosynteny) over substantial periods of time. For example, tephritid fruit flies have maintained chromosome arms, known as Muller elements (Schaeffer 2018), over at least 60 million years (My) (Sved et al. 2016). Conservation of chromosome structure is even more striking in mosquitos, where chromosome arms have been maintained for at least 150 My despite substantial changes in genome size (Dudchenko et al. 2017). Among Lepidoptera, the ancestral chromosome complement has largely been maintained over 140 My, and where changes in karyotype have occurred, they have been driven by chromosome fusion and fission events that maintain ancestral chromosome fragments (d'Alençon et al. 2010; Heliconius Genome Consortium et al. 2012; Ahola et al. 2014; Davey et al. 2015). The green-veined white butterfly (*Pieris napi*) appears to be one of the few lepidopteran exceptions, as a chromosome-scale reference genome for this insect has recently revealed extensive genome rearrangement despite having a chromosome number similar to model species (Hill et al. 2019).

Nonetheless, chromosome number is highly variable across insects as a whole (Blackmon et al. 2017), suggesting that the conserved genome structures of Diptera and Lepidoptera cannot be used as models for all insects. A dramatic example of this can be found in aphids—an important group of hemimetabolous sap-sucking plant pests belonging to the insect order Hemiptera—where characterized karyotypes vary from $2n = 4$ (two pairs of diploid chromosomes) to $2n = 72$ (Blackman 1980). This variation occurs between closely related species, and even within species, suggesting a high rate of chromosome evolution (Blackman 1971; Panigrahi and Patnaik 1991; Blackman et al. 2000; Monti et al. 2012; Mandrioli et al. 2014; Manicardi, Nardelli, et al. 2015).

Aphid chromosome structure and life cycle may contribute to the rapid evolution of diverse karyotypes (Blackman 1980). First, aphids and other Hemiptera have holocentric chromosomes that lack localized centromeres (Hughes-Schrader and Schrader 1961; Melters et al. 2012; Drinnenberg et al. 2014). Instead, spindle fibers attach diffusely across the chromosome during meiosis and mitosis (Ris 1942, 1943). As such, both products of a chromosomal fission event can undergo replication, whereas in species with localized centromeres, the fragment lacking the centromere would be lost (Ris 1942; Schrader 1947). Second, aphids have an unusual reproductive mode—cyclical parthenogenesis—where they reproduce clonally via apomictic parthenogenesis during the spring, summer, and autumn, followed by a sexual stage that produces overwintering eggs from which asexually reproducing females hatch (Dixon 1977). Clonal lineages can persist for long periods without sexual reproduction and some species have become obligately asexual (Moran 1992; Simon et al. 2002). These bouts of prolonged asexuality, combined with males being derived from an asexual lineage, may enable rearranged karyotypes to persist and potentially contribute to speciation events, thus facilitating the evolution of diverse karyotypes.

Genome sequencing of a small number of aphid species has also revealed dynamic patterns of genome evolution, with extensive gene duplication having occurred throughout aphid diversification (IAGC 2010; Mathers et al. 2017; Thorpe et al. 2018; Li et al. 2019; Fernández et al. 2020; Julia et al. 2020). However, at the time this study started, aphid genome assemblies were highly fragmented (although see Li et al. [2019] and Chen et al. [2019]) and chromosome-scale genome assemblies had not yet been analyzed to assess the evolution of aphid karyotypes and how this compares with diverse Hemiptera.

Here, we generated high-quality chromosome-scale genome assemblies of two extensively studied aphid species: the green peach aphid *Myzus persicae*, a model generalist aphid and major crop pest (Mathers et al. 2017), and the pea aphid *Acyrtosiphon pisum*, a model for speciation genomics and basic aphid biology (Hawthorne and Via 2001; Brisson and Stern 2006; Peccoud et al. 2009; Pecoud and Simon 2010; Nouhaud et al. 2018). Comparison of these new aphid assemblies with a previously published chromosome-scale assembly of the corn-leaf aphid *Rhopalosiphum maidis* (Chen et al. 2019) showed that, over the last ~30 My, aphid autosomes have undergone dramatic reorganization. In contrast, gene content of the aphid sex (X) chromosome remained unchanged.

While this work was under review (Mathers et al. 2020b), Li et al. (2020) also found extensive autosome reorganization in aphids by comparing *A. pisum* and *R. maidis* genomes and provided evidence that chromosome evolution of aphids is distinct from that of a psyllid, an obligate sexually reproducing species that, like aphids, belongs to the suborder Sternorrhyncha, within Hemiptera. In this study, we extend the analyses of hemipteran genome evolution beyond Sternorrhyncha by including the recently released chromosome-scale assemblies of *Rhodnius prolixus* (obtained from the DNA Zoo; Dudchenko et al. 2017) and *Triatoma rubrofasciata* (Liu et al. 2019), two blood-feeding heteropterans with obligate sexual life cycles whose divergence from Sternorrhyncha represents a basal split in extant Hemiptera (Johnson et al. 2018). By comparing across Hemiptera, we find evidence to support the ancient conservation of hemipteran X chromosome gene content and reveal divergent patterns of autosome evolution between aphids and the two investigated Heteroptera. Furthermore, using our new high-quality genome assemblies of *M. persicae* and *A. pisum*, we investigate the evolution and genome-wide distribution of aphid transposable elements (TEs), finding an association between the accumulation of specific repeat classes and autosomal synteny breakpoint regions as well as revealing new insights into aphid X chromosome dynamics.

Results and Discussion

Chromosome-Scale Assemblies of the *M. persicae* and *A. pisum* Genomes

High-quality, chromosome-scale, genome assemblies of *M. persicae* (clone O) and *A. pisum* (clone JIC1) were generated using a combination of Illumina short-read sequencing,

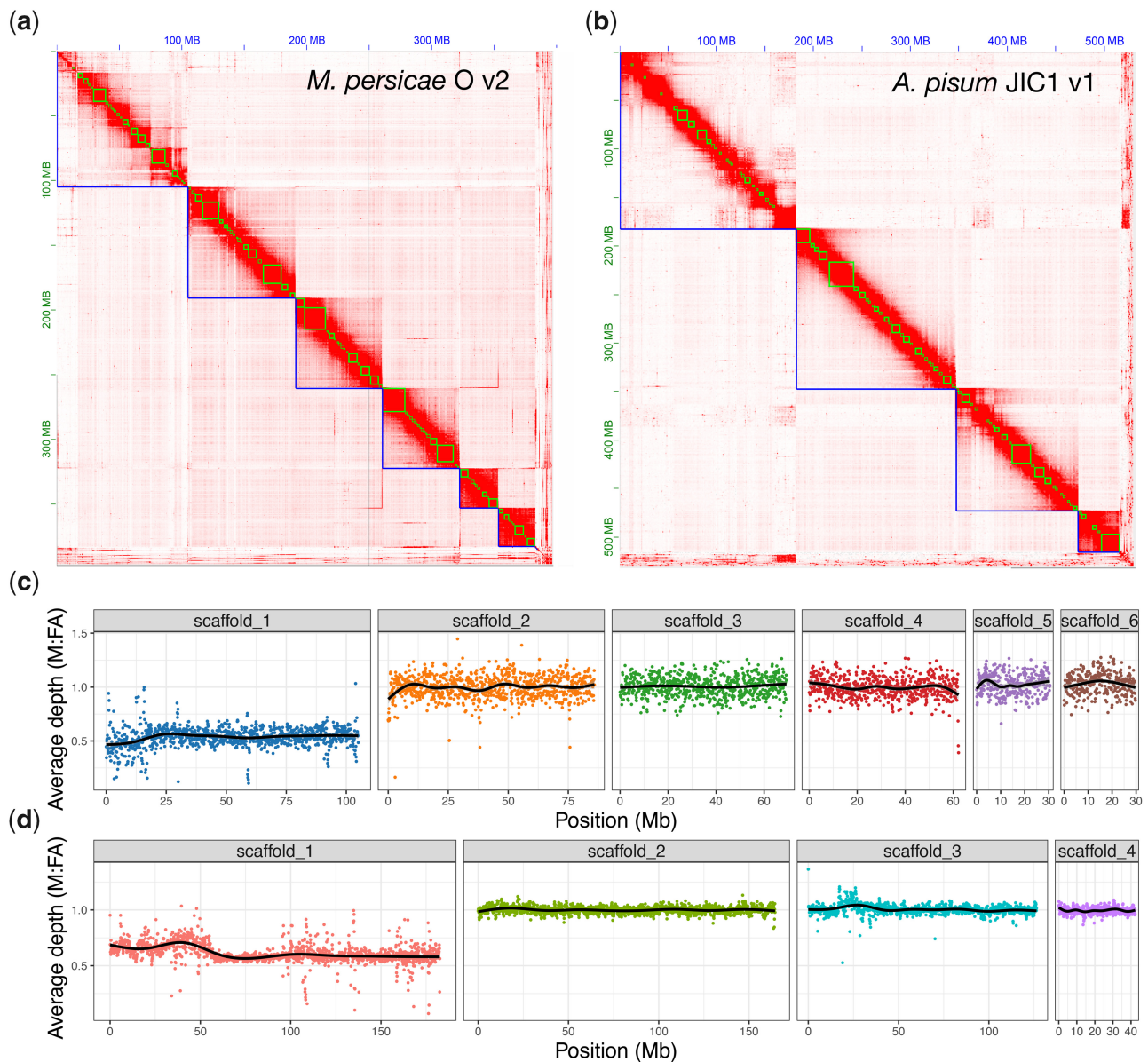


Fig. 1. Chromosome-scale genome assemblies of *Myzus persicae* and *Acyrtosiphon pisum*. (a) Heatmap showing frequency of HiC contacts along the *M. persicae* clone O v2 (MperO_v2) genome assembly. Blue lines indicate super scaffolds and green lines show contigs. Genome scaffolds are ordered from longest to shortest with the x and y axis showing cumulative length in millions of base pairs (Mb). (b) As for (a) but showing HiC contacts along the *A. pisum* JIC1 v1 (ApisJIC1) genome assembly. In this instance, green lines indicate corrected scaffolds from the input assembly which was scaffolded with 10X Genomics linked reads prior to chromosome-scale scaffolding with HiC. (c) Male (M) to asexual female (FA) coverage ratio of *M. persicae* clone bisulfite sequencing genomic reads in 100-kb fixed windows across MperO_v2 chromosome-length scaffolds. The black line indicates the LOESS smoothed average. (d) As for (c) but showing the M to FA coverage ratio of *A. pisum* clone AL4 genomic reads across ApisJIC1 chromosome-length scaffolds.

Oxford Nanopore long-read sequencing, 10X Genomics linked reads (for *A. pisum*), and in vivo chromatin conformation capture (HiC) (fig 1a and b). These new genome assemblies provide significant increases in contiguity compared with previously published assemblies at both the contig and scaffold level (table 1 and supplementary fig. 1, Supplementary Material online). For *M. persicae*, we report the first chromosome-scale genome assembly of this species with 97% of the assembled content contained in six scaffolds corresponding to the haploid chromosome number of this species (Blackman 1980). Compared with the original

assembly of *M. persicae* clone O (Mathers et al. 2017), contig number is reduced from 23,616 to 915 and contig N50 is increased by 707% (59 kb vs. 4.17 Mb). For *A. pisum*, 98% of the assembled content was placed into four scaffolds corresponding to the haploid chromosome number of this species (Blackman 1980). Compared with a recently rescaffolded reference assembly of *A. pisum* dubbed AL4 (Li et al. 2019), we place an additional 14% (98% vs. 86%) of the *A. pisum* genome into chromosomes, reduce the number of contigs from 68,186 to 2,298, and increase contig N50 by 1,667% (0.03 Mb vs. 0.53 Mb). K-mer analysis of each assembly versus Illumina

Table 1. Genome Assembly and Annotation Statistics for *Acyrtosiphon pisum*, *Myzus persicae*, and *Rhopalosiphum maidis*.

Species	<i>A. pisum</i>	<i>A. pisum</i>	<i>A. pisum</i>	<i>M. persicae</i>	<i>M. persicae</i>	<i>R. maidis</i>
Assembly	LSR1 v2	AL4 v1	JIC1 v1	O v1.1	O v2	BTI-1 v1
Sequencing approach ^a	S + IL + MP	HiC ^b	10X + ONT + HiC	IL + MP	IL + ONT + HiC	IL + PB + HiC
Base pairs (Mb)	541.68	541.12	525.80	354.7	395.14	326.02
% Ns	7.71	7.65	0.08	3.26	0.10	0.01
Number of contigs ^c	60,596	68,186	2,298	23,616	915	960
Contig N50 (Mb) ^c	0.03	0.03	0.53	0.06	4.17	9.05
Number of scaffolds	23,924	21,919	558	13,407	360	220
Scaffold N50 (Mb)	0.52	132.54	126.6	0.16	69.48	93.3
% of assembly in chromosome-length scaffolds	0	85.96	98.20	0	97.06	98.37
Protein-coding genes	36,939		30,784	18,433	27,663	17,629
Transcripts	36,939		34,135	30,247	31,842	17,629
Reference	IAGC (2010)	Li et al. (2019)	This study	Mathers et al. (2017)	This study	Chen et al. (2019)

^aS, Sanger; IL, Illumina short reads; MP, Illumina mate-pairs; 10X, 10X Genomics linked reads; HiC, high-throughput chromatin conformation capture; ONT, Oxford Nanopore long reads; PB, PacBio long reads.

^bIn vitro/in vivo (Dovetail Chicago) and in vivo HiC used to correct and scaffold LSR1 v2.

^cScaffolds split on runs of 10 or more Ns.

short reads shows very low levels of missing content and the absence of erroneously duplicated content due to the inclusion of haplotigs (allelic variation assembled into separate scaffolds) (supplementary fig. 2a and b, Supplementary Material online). Additionally, our *M. persicae* and *A. pisum* genome assemblies are accurate at the gene level, containing 94% and 98% of conserved Arthropoda benchmarking universal single-copy orthologs (BUSCO) genes ($n = 1,066$) as complete, single copies, respectively (supplementary fig. 3, Supplementary Material online). Therefore, the new assemblies of *M. persicae* and *A. pisum* are contiguous, accurate, and complete.

Using our improved *M. persicae* and *A. pisum* genome assemblies, we annotated protein-coding genes in each species using evidence from RNA-seq data. For *M. persicae*, we aligned 160 Gb of RNA-seq data derived from whole bodies of unwinged (apterous) asexual females, winged asexual females, winged males and nymphs, and annotated 27,663 protein-coding genes. For *A. pisum*, we annotated 30,784 protein-coding genes, incorporating evidence from 23 Gb of RNA-seq data that were also derived from multiple morphs including unwinged asexual females, sexual females and males. The completeness of the annotations reflected that of the genome assemblies, with 93% and 92% of conserved Arthropoda BUSCO genes ($n = 1,066$) found as complete, single copies, in the *M. persicae* and *A. pisum* annotations, respectively (supplementary fig. 4, Supplementary Material online).

Protein-coding gene counts for our new annotations of *A. pisum* and *M. persicae* differ from previous versions with 6,155 fewer genes annotated in *A. pisum* JIC1 compared with LSR1 v2 and 9,230 more genes annotated in *M. persicae* clone O v2 compared with v1.1 (table 1). This is not entirely unexpected as gene counts can vary substantially depending on the gene annotation strategy used (Yandell and Ence 2012; Denton et al. 2014). Indeed, our gene counts are much closer to the independent annotations of *A. pisum* LSR1 v2 and *M. persicae* clone G006 v2 carried out by Thorpe et al. (2018), who used the same annotation pipeline employed

in this study (BRAKER [Hoff et al. 2016, 2019]) and found 27,676 and 25,726 genes in *A. pisum* and *M. persicae*, respectively. Additionally, in the case of *M. persicae*, the use of additional RNA-seq data from diverse morphs sequenced for this study and elsewhere (Mathers et al. 2019) may have contributed to the discovery of additional genes. Finally, our improved genome assemblies may also contribute to the observed differences in gene count. The JIC1 v1 assembly of *A. pisum* is 15 Mb smaller than the LSR1 and AL4 assemblies (table 1) and is closer to the predicted *A. pisum* genome size (514 Mb; Wenger et al. 2020). In contrast, *M. persicae* clone O v2 contains an additional 40 Mb of sequence compared with v1.1 (table 1) and is also much closer to the predicted *M. persicae* genome size (409 Mb; Wenger et al. 2020).

Identification of the Aphid Sex (X) Chromosome

To identify the X chromosome, we aligned the genomic DNA Illumina reads derived from asexual female and male morphs and calculated the male to asexual female coverage ratio in 100-kb fixed windows along each chromosome. Because sex is determined by random loss of one copy of the X chromosome in aphids (Wilson et al. 1997), with males carrying a single copy of the X chromosome, males should have half the coverage of females for the X chromosome and equivalent coverage for autosomes (Jaquiéry et al. 2018). In agreement with cytological analysis of *M. persicae* and *A. pisum* (Manicardi, Mandrioli, et al. 2015), we find that the longest scaffold in their respective assemblies has the expected coverage pattern of an X chromosome along its full length (fig. 1c and d). The remaining chromosomes do not deviate from the expected male to asexual female coverage ratio of 1:1, indicating an absence of X chromosome–autosome chimeras. Alignment of *A. pisum* JIC1 with the AL4 assembly and a previously published microsatellite linkage map (Jaquiéry et al. 2014) also confirms the identity of the *A. pisum* X chromosome as scaffold 1 and, overall, JIC1 v1 is in broad agreement with AL4 with the exception of a possible inversion at the beginning of scaffold 3 that may represent true

biological variation or an assembly error in JIC1 v1 (supplementary fig. 5, Supplementary Material online). Importantly, we assemble and place an additional 50 Mb of the X chromosome in the JIC1 genome assembly compared with AL4, where the X chromosome is only the third longest scaffold and many additional genomic scaffolds with X-chromosome-like coverage patterns are unplaced (Li et al. 2019). This is likely due to improved resolution and representation of repetitive elements in JIC1 due to the use of long-read sequence data for de novo assembly. Indeed, for both *M. persicae* and *A. pisum*, we annotate a greater total length of repetitive DNA in our new assemblies than the previous versions that were based on short-read sequencing (*M. persicae* clone O: v1.1 = 57 Mb [16% of total assembly content], v2 = 88 Mb [22%]; *A. pisum*: AL4 = 154 Mb [29%], JIC1 = 178 Mb [34%]; supplementary fig. 6, Supplementary Material online).

Extensive Autosomal Genome Rearrangement in Aphids

To investigate aphid chromosome evolution, we identified syntenic genomic regions between *M. persicae*, *A. pisum*, and the published chromosome-scale assembly of *R. maidis* (Chen et al. 2019) using MCScanX (Wang et al. 2012), which identifies blocks of colinear genes (supplementary table 1, Supplementary Material online). *Myzus persicae* and *A. pisum* both belong to the aphid tribe Macrosiphini and diverged ~22 Ma, whereas *R. maidis* belongs to Aphidini and diverged from *M. persicae* and *A. pisum* ~33 Ma (fig. 2a). Assessment of chromosomal rearrangements shows a lack of large-scale rearrangements between the X chromosome and the autosomes for any of the aphid species analyzed, whereas aphid autosomes have undergone extensive structural change with many rearrangements between chromosomes (fig. 2c and d). Comparison between *M. persicae* and *A. pisum* within the tribe Macrosiphini reveals the signature of several chromosome fusion or fission events between autosomes that have occurred within the last 22 My (fig. 2c). For example, *M. persicae* scaffolds 4 and 5 are homologous to *A. pisum* scaffold 3, with the breakpoint clearly delineated. Comparing the more divergent species pair of *M. persicae* and *R. maidis*, which belong to Macrosiphini and Aphidini respectively, reveals highly rearranged autosomes with no clear homology (fig. 2d). This is also the case when comparing *R. maidis* to *A. pisum*, despite both species having the same $2n = 8$ karyotype (supplementary fig. 7, Supplementary Material online), further supporting high levels of rearrangement. Similar results were obtained by mapping orthologs independently identified based on phylogenomic analysis of gene trees to *M. persicae* chromosomes (supplementary fig. 8 and table 2a and b, Supplementary Material online). In total, we identified 11,372 chromosomally placed one-to-one orthologs between *M. persicae* and *A. pisum* (41% of *M. persicae* genes) and 9,594 between *M. persicae* and *R. maidis* (35% of *M. persicae* genes). Using these data, we confirm that the aphid X chromosome is recalcitrant to translocations with the autosomes, with 93% (1,972/2,125) and 96% (1,388/1,452) of orthologs conserved on the X chromosome between *M. persicae* and *A. pisum* and

between *M. persicae* and *R. maidis*, respectively. Taken together, our results show that the aphid X chromosome has been maintained for at least 33 My in contrast to extensive autosomal rearrangements.

Divergent Patterns of Chromosome Evolution across Hemiptera

To investigate how aphid chromosome rearrangements compare with those of other hemipterans, we took advantage of two recently released chromosome-scale assemblies of the blood-feeding species *Rhod. prolixus* (obtained from the DNA Zoo; Dudchenko et al. 2017) and *T. rubrofasciata* (Liu et al. 2019). Both species belong to the hemipteran family Reduviidae and diverged from the aphid lineage ~386 Ma (fig. 2a), representing a basal split in extant Hemiptera (Johnson et al. 2018). Unlike aphids, most Reduviidae have an XY chromosomal sex determination system (male = XY, female = XX) which is thought to be the ancestral state of Hemiptera (Blackmon et al. 2017) and reproduce exclusively through sexual reproduction. In some species, complex sex determination systems have been described with multiple X chromosomes (Ueshima 1966; Panzera et al. 1996). *Triatoma rubrofasciata* is one such species and has an X_1X_2Y male karyotype (Manna 1950). Multiple X chromosome systems in *Triatoma* are thought to be the result of X chromosome fragmentation events (Ueshima 1966), we also examine this hypothesis here.

In striking contrast to aphids (fig. 2c and d), *Rhod. prolixus* and *T. rubrofasciata* have highly conserved synteny and an absence of translocation events between chromosomes (fig. 2e), despite being almost twice as divergent at the sequence level as the most divergent aphid comparison (fig. 2b; median synonymous site divergence: *M. persicae* vs. *R. maidis* = 34%, *T. rubrofasciata* vs. *Rhod. prolixus* = 60%). In total, just two chromosome fusion or fission events are detectable, one involving *Rhod. prolixus* chromosome 6 (Rp6) and a second involving the X chromosome (Rp10). The latter is likely an X chromosome fission in the *T. rubrofasciata* lineage which has led to the multiple X chromosome sex determination system observed in this species, supporting the hypothesis proposed by Ueshima over half a century ago (Ueshima 1966). For both the *M. persicae*–*A. pisum* comparison and the *T. rubrofasciata*–*Rhod. prolixus* comparison, synteny block size is positively correlated with chromosome length (fig. 2f). This relationship breaks down for the *M. persicae*–*R. maidis* comparison, again highlighting high rates of genome rearrangement in aphids. Indeed, despite higher sequence-level divergence, autosomal synteny blocks in Reduviidae are significantly larger than those identified between the most divergent aphid pair of *M. persicae* and *R. maidis* (Wilcoxon rank-sum test, $W = 19,894$, $P = 0.02$; fig. 2g) and are similar in size to those identified between the more closely related pair of *M. persicae* and *A. pisum* (Wilcoxon rank-sum test, $W = 19,086$, $P = 0.71$). This relationship is reversed for synteny blocks on the X chromosome which are significantly larger in aphids than Reduviidae (fig. 2g), whether comparing to *M. persicae*–*A. pisum* synteny blocks (Wilcoxon rank-sum test: $W = 783$, $P = 7.55 \times 10^{-5}$) or *M. persicae*–*R. maidis*

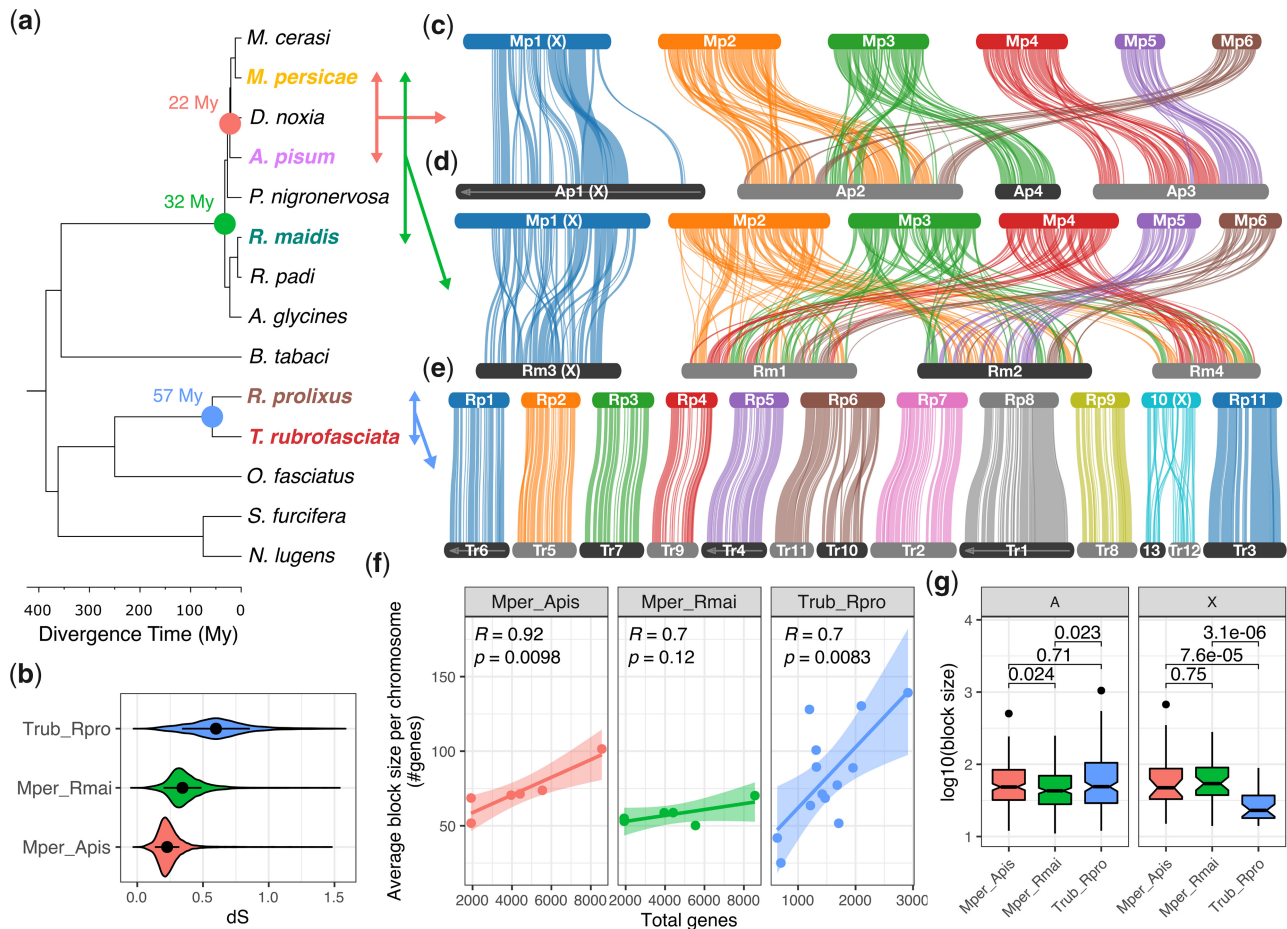


Fig. 2. Divergent patterns of chromosome evolution across Hemiptera. (a) Time calibrated phylogeny of Hemiptera based on a concatenated alignment of 785 proteins conserved in all species. Divergence times were estimated using nonparametric rate smoothing with calibration nodes specified based on Johnson et al. (2018). Species with chromosome-scale genome assemblies are colored and divergence times between focal species are highlighted with colored circles. (b) Synonymous site divergence rate (dS) between *Triatoma rubrofasciata* and *Rhodnius prolixus* (blue), *Myzus persicae* and *Rhopalosiphum maidis* (green), and *M. persicae* and *Acyrtosiphon pisum* (red) based on 9,087, 7,965, and 9,290 syntenic one-to-one orthologs, respectively. Black circles and whiskers show median and interquartile range, respectively. (c–e) Pairwise synteny relationships within aphids (c and d) and Reduviidae (e) are mapped onto the phylogeny of Hemiptera. Links indicate the boundaries of syntenic gene blocks identified by MCScanX and are color coded by *M. persicae* (c and d) or *Rhod. prolixus* (e) chromosome ID. *Acyrtosiphon pisum* (c) and *R. maidis* (d) chromosomes are ordered based on *M. persicae*, and *T. rubrofasciata* (e) chromosomes are ordered according to *Rhod. prolixus*. Arrows along chromosomes indicate reverse complement orientation relative to the focal species. Regions of chromosomes not joined by links lack detectable synteny at the resolution of our analysis. (f) The relationship between average synteny block size per chromosome (y axis) and chromosome size (x axis; measured as the total number of genes per chromosome). Trend lines show linear regression with 95% confidence intervals. For each comparison, the Pearson correlation coefficient (R) is given. (g) The size of MCScanX synteny blocks (measured in the number of genes within each block) located either on autosomes (A) or the X chromosome (X) for comparisons shown in (c)–(e). Numbers above comparisons show P values from Wilcoxon rank-sum tests.

synteny blocks (Wilcoxon rank-sum test: $W = 1155$, $P = 3.08 \times 10^{-6}$). Taken together, these results show divergent patterns of both inter- and intra-chromosomal rearrangement rates between aphids and Reduviidae, and that aphid diversification is associated with dynamic changes in autosome structure.

TEs Are Enriched in Synteny Breakpoint Regions

Genome rearrangements may occur through nonallelic homologous recombination between repetitive elements (Mieczkowski et al. 2006; Chénais et al. 2012; Startek et al. 2015; Piazza and Heyer 2019). We hypothesized that

repetitive elements are associated with the observed elevated rate of autosomal rearrangements in aphids. To test this, we compared TE content of autosomal synteny breakpoint regions (hereafter referred to as breakpoint regions) with those of conserved synteny blocks for the most recently diverged aphid species pair (i.e., *M. persicae* and *A. pisum*; fig. 2c). In total, breakpoint regions (excluding chromosome ends) span 34.5 Mb (12.4%) of autosomal sequence in *M. persicae* with an average length of 184 kb ($n = 187$, min = 60 bp, max = 2 Mb). TEs are highly enriched within breakpoint regions, accounting for 31.5% of all breakpoint region sequence compared with 17.9% in syntenic regions

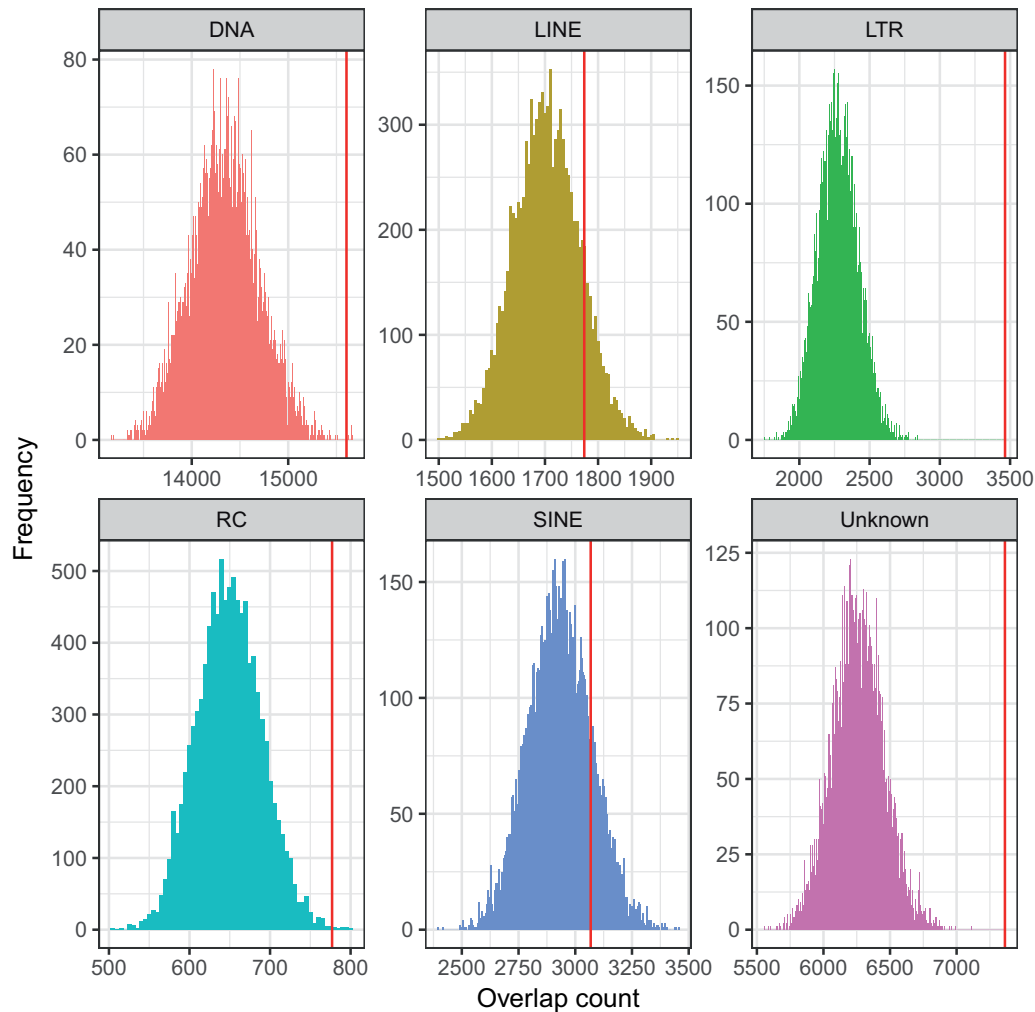


Fig. 3. TEs are enriched within *Myzus persicae*–*Acyrtosiphon pisum* autosomal synteny breakpoint regions in the *M. persicae* clone O genome. Histograms show the distribution of TE counts (by class) in 10,000 randomized sets of autosomal regions with the same size distribution as observed *M. persicae*–*A. pisum* autosomal synteny breakpoint regions. Red lines indicate real observed values for each TE class within autosomal synteny breakpoint regions which shows that DNA transposons (DNA), long terminal repeat retrotransposons (LTR), rolling-circle Helitron transposons (RC), and unidentified transposons (Unknown) are significantly enriched in the breakpoint regions. The long and short interspersed nuclear elements (LINE and SINE, respectively) are not enriched.

(supplementary table 3a, Supplementary Material online). TE content within breakpoint regions is nonrandom, with long terminal repeat (LTR) retrotransposons being most strongly enriched relative to random expectation (fig. 3 and supplementary table 3a, Supplementary Material online; permutation test: $P < 0.0001$). Indeed, despite representing only 12.4% of the genome, 29.5% of all autosomal LTR sequences are located within breakpoint regions, an enrichment of 2.38 times (supplementary table 3a, Supplementary Material online). Similar results were also found using the *A. pisum* JIC1 assembly as reference, with autosomal breakpoint regions strongly enriched for TEs compared with synteny blocks (44.6% vs. 28.1% TE content; supplementary table 3b, Supplementary Material online). As for *M. persicae*, the strongest enrichment of TEs within breakpoint regions was found for LTR elements (supplementary table 3b and fig. 9, Supplementary Material online; permutation test: $P < 0.0001$). Taken together, our results suggest that TE insertions may provide substrate for aphid genome rearrangement events.

Conservation of Hemipteran X Chromosome Gene Content

To test the hypothesis that the X chromosome is conserved across Hemiptera (Pal and Vicoso 2015), we compared our chromosome-scale assembly of *M. persicae* with *Rhod. prolixus*. We failed to identify syntenic blocks of genes between the two genome assemblies using MCScanX, probably due to the large evolutionary distance between *M. persicae* and *Rhod. prolixus* (386 My). Nonetheless, 6,191 one-to-one orthologs were identified between the two species (22% of *M. persicae* genes), 5,992 (97%) of which are anchored to chromosomes in both species. Using these orthologs, we find that the *M. persicae* X chromosome is significantly enriched for genes located on the *Rhod. prolixus* X chromosome (Rp10) (binomial test: Benjamini–Hochberg [BH] corrected $P = 3.91 \times 10^{-13}$; fig. 4a and c and supplementary fig. 10, Supplementary Material online), suggesting that the aphid and *Rhodnius* X

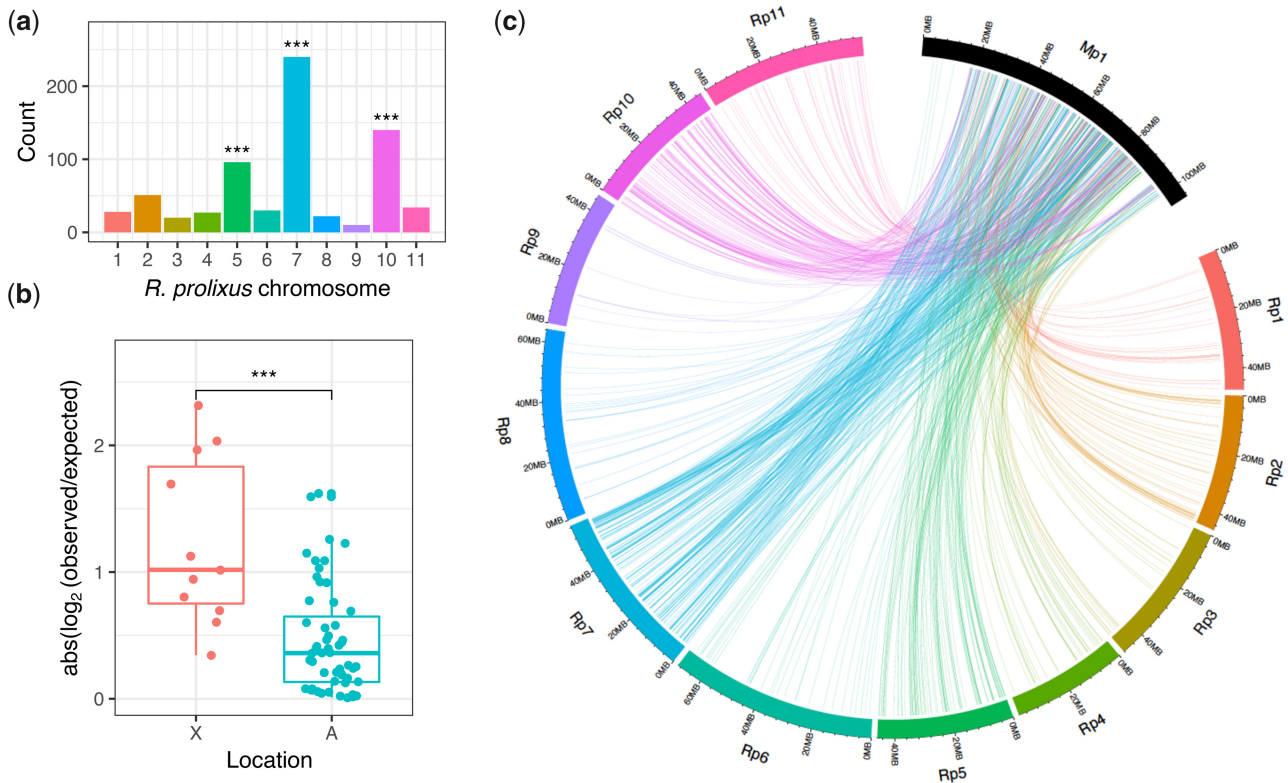


Fig. 4. Ortholog mapping between the aphid *Myzus persicae* and the kissing bug *Rhodnius prolixus*. (a) Counts of *Rhod. prolixus* chromosomal location for 698 *M. persicae*–*Rhod. prolixus* 1:1 orthologs located on the *M. persicae* X chromosome (scaffold_1). Stars above bars indicate significant enrichment of a specific *Rhod. prolixus* chromosome after correcting for multiple testing (binomial test: BH corrected $P < 0.05$). (b) Absolute odds ratios ($\log_2[\text{observed/expected}]$) for *Rhod. prolixus* chromosomal enrichment on the *M. persicae* X chromosome and *M. persicae* autosomes. Each dot shows the odds ratio for a specific *Rhod. prolixus* chromosome. ***Wilcoxon rank-sum test $W = 517$, $P = 2.31 \times 10^{-4}$. (c) Chord diagram showing links between the *M. persicae* X chromosome (shown as Mp1) and the *Rhod. prolixus* chromosomes for 1:1 orthologs. Rp10 is the *Rhod. prolixus* X chromosome, the *Rhod. prolixus* Y chromosome is not assembled.

chromosomes are homologous. Furthermore, absolute enrichment (and hence depletion) ratios of orthologs from specific *Rhod. prolixus* chromosomes were significantly higher for the *M. persicae* X chromosome than the autosomes (Wilcoxon rank-sum test: $W = 517$, $P = 2.31 \times 10^{-4}$; fig. 4b and supplementary table 4, Supplementary Material online), indicating that elevated conservation of the X chromosome, relative to autosomes, extends across Hemiptera. We also find that the *M. persicae* X chromosome is significantly enriched for genes that map to *Rhod. prolixus* autosomes Rp7 (binomial test: BH corrected $P < 1.00 \times 10^{-16}$) and Rp5 (binomial test: BH corrected $P = 3.91 \times 10^{-13}$) (fig. 4a and c). This suggests that the ancestral hemipteran X chromosome may have been fragmented in the *Rhod. prolixus* lineage or, alternatively, the aphid X chromosome may be a product of an ancient chromosome fusion event.

The Aphid X Chromosome Is Repetitive, Depleted in Expressed Genes, and Rapidly Evolving

Conservation of aphid X chromosome gene content is remarkable given its dynamic genomic substrate. In *M. persicae* and *A. pisum*, the X chromosome is significantly more repetitive than the autosomes and significantly depleted in expressed genes (fig. 5a–d). Across the *M. persicae* X chromosome, 27% of bases are annotated as

TEs compared with 19% in autosomes ($\chi^2 = 3,486,014$, $df = 1$, $P < 2.2 \times 10^{-16}$). The *A. pisum* X chromosome is even more repetitive, with 42% of bases annotated as TEs compared with 29% in autosomes ($\chi^2 = 8,455,518$, $df = 1$, $P < 2.2 \times 10^{-16}$). The ends of the X chromosome in both *M. persicae* and *A. pisum* appear to be gene expression deserts with low numbers of expressed genes relative to the autosomes and to the central regions of the X chromosome (fig. 5a and b). These gene-poor regions have significant reduction in the density of expressed genes toward the telomeres (*M. persicae*: Pearson correlation [R] = -0.46 , $P = 6.4 \times 10^{-7}$; *A. pisum*: $R = -0.46$, $P = 5.1 \times 10^{-11}$; supplementary figs. 11 and 12, Supplementary Material online). This reduction is associated with significant increases in the densities of DNA transposons (*M. persicae*: $R = 0.51$, $P = 1.9 \times 10^{-8}$; *A. pisum*: $R = 0.63$, $P < 2.2 \times 10^{-16}$), LTR retrotransposons (*M. persicae*: $R = 0.52$, $P = 1.0 \times 10^{-8}$; *A. pisum*: $R = 0.46$, $P = 4.4 \times 10^{-11}$), and rolling-circle Helitron transposons (*M. persicae*: $R = 0.50$, $P = 6.5 \times 10^{-8}$; *A. pisum*: $R = 0.38$, $P = 1.2 \times 10^{-7}$) (fig. 5a and b and supplementary figs. 11 and 12, Supplementary Material online). There is also a weak but significant increase in long interspersed nuclear elements (LINE) toward the ends of the X chromosome in both species (*M. persicae*: $R = 0.20$, $P = 0.04$; *A. pisum*: $R = 0.16$, $P = 0.029$).

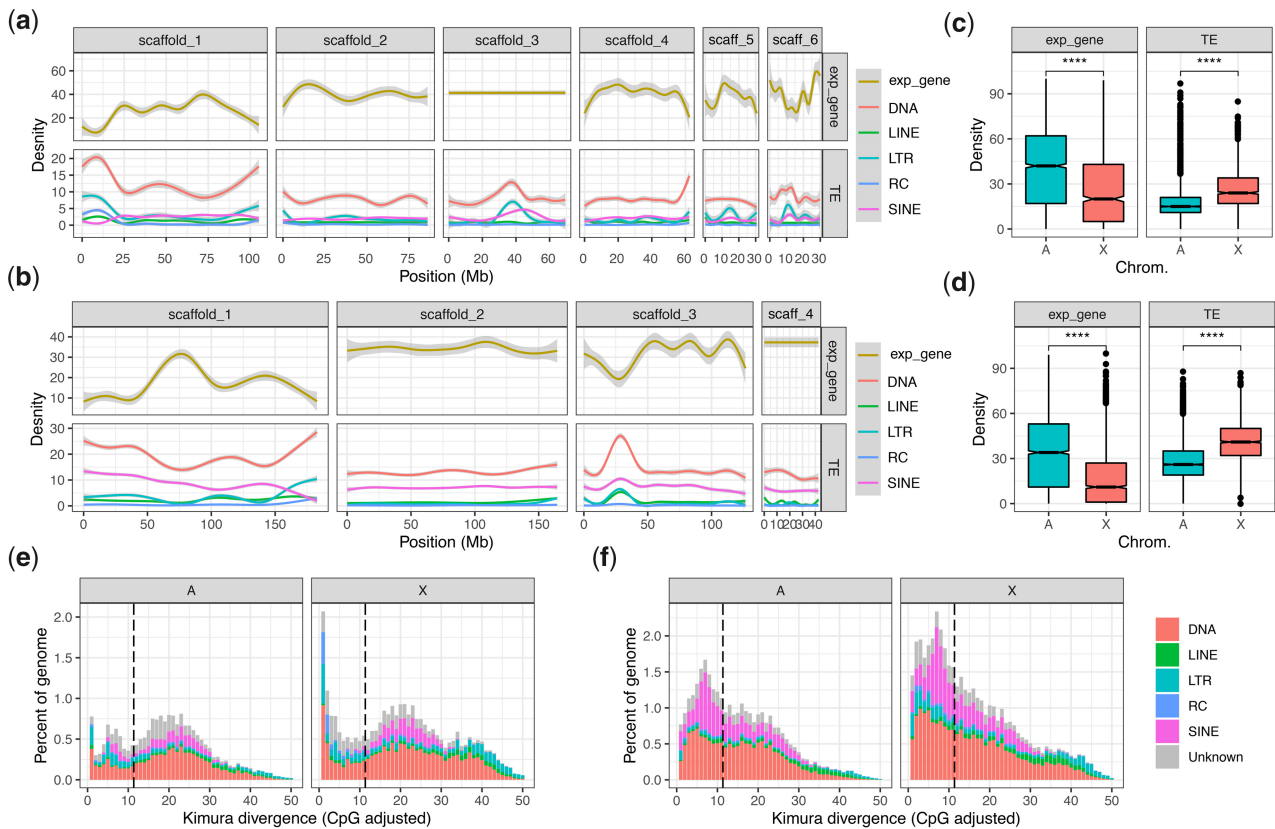


Fig. 5. The aphid X chromosome is repetitive and depleted in expressed genes. (a) The density of expressed genes (expr_gene) and TEs across *Myzus persicae* clone O v2 chromosome-length scaffolds. Genes were classified as expressed if they had an estimated read count >4 in at least 12/24 *M. persicae* morph RNA-seq samples (see fig. 6). Lines show LOESS smoothed averages of 100-kb fixed windows. For detailed plots showing all data points for each feature class, see supplementary figures 14 and 15, Supplementary Material online. DNA, DNA transposons; LINE, long interspersed nuclear element; LTR, long terminal repeat retrotransposons; RC; rolling-circle transposons; SINE, short interspersed nuclear elements. (b) As for (a) but showing TEs and expressed genes across *Acyrthosiphon pisum* chromosome-length scaffolds. Genes were classified as expressed if they had an estimated read count >4 in at least 3/6 *A. pisum* morph RNA-seq samples from Jaquiéry et al. (2013). (c) Box plots showing median density of expressed genes and TEs in 100-kb fixed windows across *M. persicae* autosomes and the X chromosome. The X chromosome has significantly lower gene density (Wilcoxon rank-sum test: $W = 1,934,963$, $P < 2.2 \times 10^{-16}$) and significantly higher TE density (Wilcoxon rank-sum test: $W = 786,210$, $P < 2.2 \times 10^{-16}$) than the autosomes. (d) Box plots showing median density of expressed genes and TEs in 100-kb fixed windows across *A. pisum* clone JIC1 autosomes and the X chromosome. The X chromosome has significantly lower gene density (Wilcoxon rank-sum test: $W = 16,062,992$, $P < 2.2 \times 10^{-16}$) and significantly higher TE density (Wilcoxon rank-sum test: $W = 6,340,780$, $P < 2.2 \times 10^{-16}$) than the autosomes. (e) Stacked histograms showing the age distribution of TEs located on *M. persicae* clone O autosomes (A) and the X chromosome (X). TE families are grouped as for (a) and (b). The dashed black line indicates half the median synonymous site divergence (11.35%) between *M. persicae* and *A. pisum* one-to-one orthologs and is a proxy for the divergence time, that is, TE insertions with lower divergence from their respective consensus sequence than this point likely arose after *M. persicae* and *A. pisum* diverged. (f) As for (e) but for *A. pisum* clone JIC1.

The invasion of the aphid X chromosome by TEs appears to be ongoing, with many young TEs annotated in both *M. persicae* and *A. pisum* (fig. 5e and f). This is particularly pronounced in *A. pisum* where X chromosome TE dynamics have had a substantial influence on the size of the *A. pisum* genome. Overall, the *A. pisum* JIC1 assembly is 131 Mb (33%) larger than the *M. persicae* clone O v2 assembly (table 1; 526 vs. 395 Mb). Strikingly, 59% of this difference is due to the size of the X chromosome, which is 78 Mb larger (74%) in *A. pisum* (X chromosome = 183 Mb) than *M. persicae* (X chromosome = 105 Mb). Given we can rule out X chromosome-autosome fusions in *A. pisum* based on our synteny analysis (fig. 1c), the difference in X chromosome size is the product of expansion in *A. pisum* and/or contraction in *M. persicae*. Although both of these factors likely play a role, our analysis of *A. pisum* TE

dynamics indicates that lineage-specific TE expansion in *A. pisum* accounts for a substantial proportion of the observed size difference compared with *M. persicae*. We base this conclusion on the relatively young age of the TEs in the X chromosome of *A. pisum*. Using the conservative estimate that the substitution rate of TE insertions is equivalent to that of synonymous sites in protein-coding genes (i.e., approximately neutral), the *A. pisum* X chromosome contains 41 Mb of TE insertions that likely accumulated since *A. pisum* and *M. persicae* diverged (fig. 5f; divergence from consensus < 11.35%). In other words, recent TE insertions on the *A. pisum* X chromosome account for ~53% of the X chromosome size difference compared with *M. persicae*.

As well as being repetitive, we also find that genes on the *M. persicae* X chromosome have a higher rate of evolution

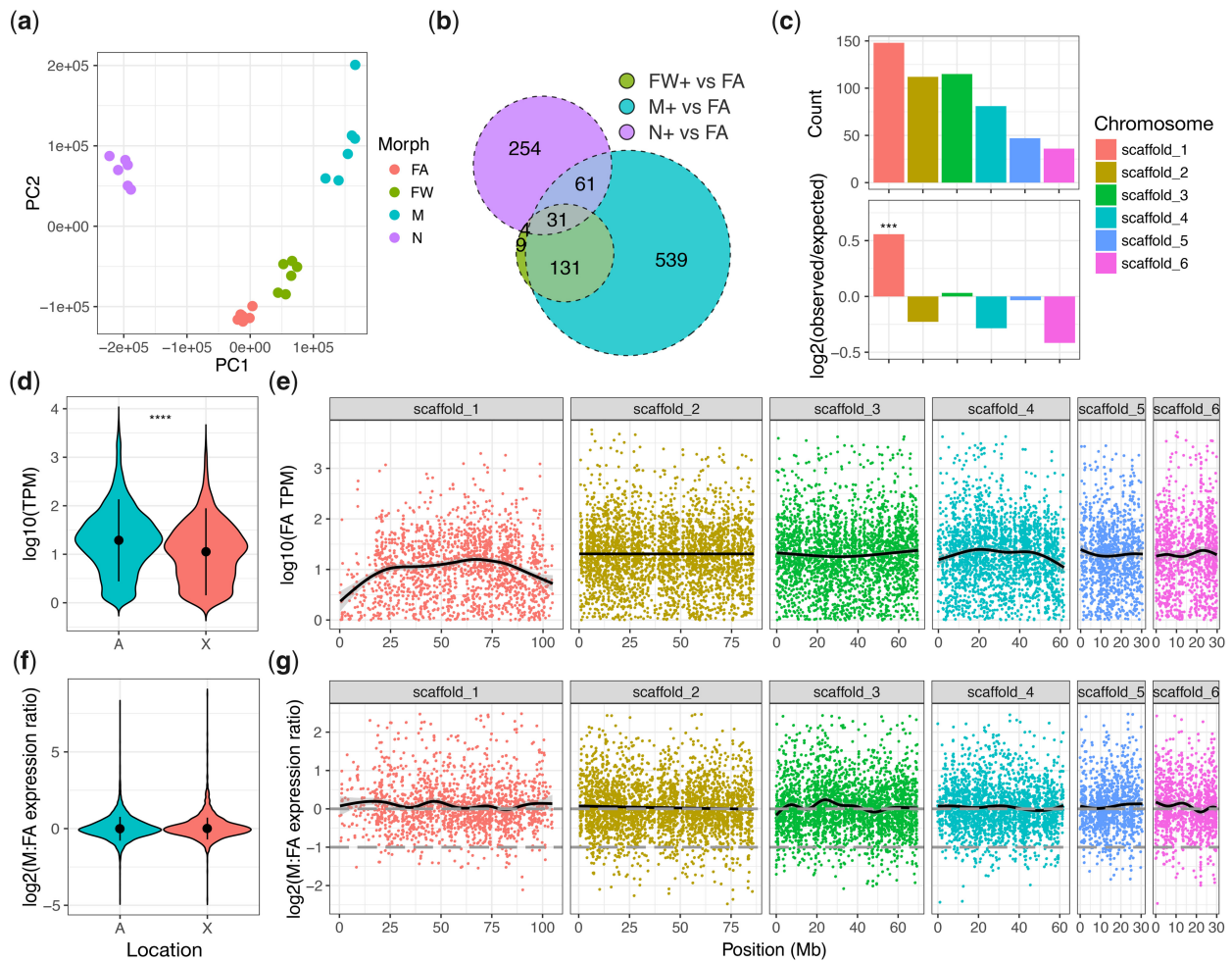


FIG. 6. Patterns of gene expression in *Myzus persicae* morphs and along *M. persicae* clone O v2 chromosome-length scaffolds. (a) Principle component analysis (PCA) based on RNA-seq gene expression levels in whole bodies of *M. persicae* clone O unwinged asexual females (FA), winged asexual females (FW), winged males (M), and nymphs (N). Each morph has a distinct gene expression profile with tight clustering of replicates ($n = 6$ per morph). (b) Overlap of genes upregulated in either M, FW, or N relative to FA (Sleuth likelihood ratio test: $q < 0.05$, effect size (beta) > 0.5). (c) The distribution of genes specifically upregulated in males ($n = 539$) across *M. persicae* clone O v2 chromosome-length scaffolds. Top panel shows counts of M-biased genes per scaffold. Bottom panel shows enrichment scores ($\log_2[\text{observed/expected}]$) of M-biased genes per scaffold relative to the total number of expressed genes on each scaffold (estimated read count > 4 in at least 12/24 RNA-seq samples). Significant enrichment was assessed using a binomial test ($P < 0.05$) with the number of trials equal to the count of expressed genes per scaffold and the probability of success equal to the overall proportion of M-biased genes located on chromosomes relative to the number of expressed genes on all chromosomes. Only the X chromosome is significantly enriched for M-biased genes. ***Binomial test: $P = 2.38 \times 10^{-6}$. (d) Violin plots showing the distribution of \log_{10} average expression levels (measured in TPM) in FA of expressed genes (TPM > 1) located on *M. persicae* autosomes (A) and the X chromosome (X). The X chromosome has significantly lower gene expression levels than the autosomes (Wilcoxon rank-sum test: $W = 715,820$, $P < 2.2 \times 10^{-16}$). (e) FA gene expression ratios used in (d) across *M. persicae* clone O v2 chromosome-length scaffolds. Each dot corresponds to a gene, the black line shows the LOESS smoothed average. (f) Violin plots showing the distribution of \log_2 M to FA gene expression ratios on *M. persicae* autosomes (A) and the X chromosome (X) for genes with average expression of at least 1 TPM in M and FA. Black circles and lines within the colored regions indicate the median and interquartile range, respectively. There is no significant difference between A and X (Wilcoxon rank-sum test: $W = 8,919,400$, $P = 0.10$). (g) The distribution of \log_2 M to FA gene expression ratios used in (f) across *M. persicae* clone O v2 chromosome-length scaffolds. Each dot corresponds to a gene, the black line shows the LOESS smoothed average. The dashed gray lines indicate the expected M to FA gene expression ratio given full dosage compensation ($\log_2[\text{M:FA}]$ expression = 0) and in the absence of dosage compensation ($\log_2[\text{M:FA}]$ expression = 0.5). Extremely M-biased or FA-biased genes (abs. \log_2 M:FA expression ratio > 2.5) are excluded.

(measured using the ratio of the nonsynonymous to synonymous nucleotide substitutions) than those on the autosomes (supplementary fig. 13 and table 1, Supplementary Material online), a phenomenon previously observed in *A. pisum* (Jaquière et al. 2012, 2018). Our results are therefore consistent with a “fast-X” effect operating across aphids. Stability of aphid X chromosome gene content has therefore been maintained in

the face of extensive historical, and ongoing, TE activity and high rates of sequence evolution.

Patterns of Gene Expression along the M. persicae Genome
Unlike other systems where a fast-X effect is observed (Mank et al. 2010), rapid evolution of the aphid X chromosome

cannot be explained by reduced efficacy of selection caused by a lower effective population size of the X chromosome relative to autosomes (Jaquiéry et al. 2012). This is because progeny produced by aphid sexual reproduction are exclusively female (XX) and inherit an X chromosome from both of their parents, leading to an equivalency of effective population size between the X chromosome and the autosomes (Jaquiéry et al. 2012). Rather, aphid fast-X evolution is thought to be predominantly explained by patterns of gene expression. Specifically, lower gene expression levels of X-linked genes compared with those on the autosomes, and enrichment of genes expressed in rare morphs, that is, males and sexual females, possibly driven by antagonistic selection (Jaquiéry et al. 2018). Both of these factors lead to relaxed purifying selection on X-linked genes. We examined these hypotheses using our new chromosome-scale assembly of *M. persicae* and a large gene expression data set for diverse *M. persicae* morphs. In particular, we investigated genome-wide patterns of gene expression in unwinged asexual females, winged asexual females, winged males, and unwinged asexual female nymphs (fig. 6a). We identified 5,046 differentially expressed genes between *M. persicae* morphs assuming a 5% false discovery rate (Sleuth likelihood ratio test: $q < 0.05$, absolute effect size [beta] > 0.5 relative to asexual female morphs; supplementary table 5, Supplementary Material online). Out of a total of 1,029 morph-biased genes, 539 (52.4%) are specifically upregulated in males relative to the common wingless asexual female morph (fig. 6b). These male-biased genes are significantly enriched on the *M. persicae* X chromosome (binomial test: $P = 2.38 \times 10^{-6}$; fig. 6c), confirming our previous results obtained using a fragmented genome assembly (Mathers et al. 2019) and matching patterns of male-biased gene expression observed in *A. pisum* (Jaquiéry et al. 2013; Purandare et al. 2014; Pal and Vicoso 2015). Using gene expression data for asexual females, we confirm that the X chromosome has significantly lower gene expression than the autosomes (Wilcoxon rank-sum test: $W = 715,820$, $P < 2.2 \times 10^{-16}$; fig. 6d) and that this is particularly pronounced for the 5' and 3' ends of the chromosome (fig. 6e).

Finally, we also confirm the operation of dosage compensation in *M. persicae*; despite the X chromosome being found as a single copy in males, there was no significant difference observed in the male to asexual female gene expression ratio between the X chromosome and the autosomes (Wilcoxon rank-sum test: $W = 8,919,400$, $P = 0.10$; fig. 6f and supplementary table 6, Supplementary Material online). Dosage compensation has previously been shown to operate in other Hemiptera (Pal and Vicoso 2015) and in *A. pisum* (Jaquiéry et al. 2013; Richard et al. 2017) using fragmented assemblies. Using our new chromosome-scale assembly of *M. persicae*, we are able to show that dosage compensation operates across the entire X chromosome (fig. 6g).

Conclusion

We find that three aphid species within the subfamily Aphidinae, that span ~30 My of aphid evolution, show extensive autosomal genome rearrangements. This is in contrast

to other insect genomes that have been compared thus far, including within Lepidoptera and Diptera. Furthermore, the high rate of autosomal rearrangements does not appear to be a ubiquitous feature of Hemiptera given that two other Hemiptera (*Rhod. prolixus* and *T. rubrofasciata*) have highly conserved synteny (fig. 2e). Our data support previous karyotype studies showing that chromosome numbers are highly variable among aphids (Blackman 1980). Furthermore, our data reveal that aphid chromosome number variation is not only caused by chromosome fission or fusion (i.e., macro-mutations) but also caused by interautosomal translocation events. In contrast to the autosomes, the aphid X chromosome appears to be recalcitrant to rearrangement with the autosomes, and it appears structurally highly conserved. The long-term stability of aphid X chromosome gene content is surprising, given that we observed low levels of gene expression of X-linked genes, relaxed selection on coding genes, and an accumulation of TEs. This implies that strong selection may be acting against interchromosomal rearrangements involving the X chromosome in aphids. It is possible that large-scale translocations involving the X chromosome interfere with dosage compensation, causing the misexpression of genes (Sharp et al. 2002). Alternatively, intact X chromosomes may be required for proper elimination of the X chromosome during male determination. If X chromosome conservation is not caused by natural selection, there might be an as yet unidentified process that curbs the rate of rearrangement of this chromosome.

A recent study by Li et al. (2020), published shortly after the early release of our results (Mathers et al. 2020b), also revealed high rates of autosomal genome rearrangement in aphids and conservation of the X chromosome. Li et al. (2020) compared a chromosome-scale assembly of *A. pisum* (AL4; Li et al. 2019) with the published assembly of *R. maidis* (Chen et al. 2019). Here, we generated another chromosome-scale assembly of a different *A. pisum* isolate (JIC1) using long-read sequencing, linked-read sequencing, and chromatin conformation capture (HiC). Compared with AL4, the assembly of JIC1 is more contiguous, allowing better comparison among aphid species. In particular, by using long-read sequencing, we dramatically improve the assembly of the *A. pisum* X chromosome, incorporating an additional 50 Mb of sequence. Moreover, this study included a highly contiguous chromosome-level assembly of another aphid species, *M. persicae*, which belongs to a different clade within Macrosiphini, whereas *R. maidis* belongs to the tribe Aphidini. By including more closely related aphid species, we demonstrate that the high rate of autosomal rearrangement in aphids appears to be ongoing, at least within Aphidinae (Macrosiphini + Aphidini).

Li et al. (2020) also confirm previously described features of pea aphid gene expression and genome architecture (Jaquiéry et al. 2013; Purandare et al. 2014; Richard et al. 2017), showing that the X chromosome has lower gene expression levels than the autosomes, that dosage compensation operates on X-linked genes and that the X chromosome is enriched in genes with male-biased expression. We confirm the generality of these findings using our new high-quality genome assembly

of *M. persicae* and a comprehensive transcriptomic data set of diverse *M. persicae* morphs.

With the improved long-read genome assembly of *A. pisum* and the high-quality long-read assembly of *M. persicae* in hand, we were able to carry out a detailed analysis of repeat evolution in aphids, gaining insights into both X chromosome and autosome evolution. We find that the large difference in genome size observed between *M. persicae* and *A. pisum* has been substantially influenced by recent TE activity on the *A. pisum* X chromosome. We also find evidence that repeats may be playing an important role in the high rate of genome rearrangement observed in aphids with significant enrichment of LTR retrotransposons, DNA transposons, and rolling-circle Helitron transposons found within synteny breakpoint regions.

Li et al. (2020) compared *A. pisum* (AL4) and *R. maidis* with a chromosome-level genome assembly of a psyllid (*Pachypsylla venusta*), which, like aphids, belongs to the sub-order Sternorrhyncha. This revealed low levels of synteny and distinct patterns of sex-biased gene expression and selection on the psyllid X chromosome compared with the aphid X chromosome. We extend the analysis of hemipteran chromosome evolution across the full span of the order by including two blood-feeding members of Reduviidae (Hemiptera: Heteroptera), which represent a basal split within Hemiptera relative to aphids (fig. 2a). The inclusion of these additional species reveals a surprising divergence in hemipteran autosome evolution, with high synteny observed between the two investigated Reduviidae species contrasting with extensive rearrangement in aphids. This is a significant observation as it suggests that the presence of holocentric chromosomes alone does not explain the observed high rate of autosomal genome rearrangement in aphids given that holocentricity is conserved across Hemiptera (Melters et al. 2012). Additionally, by including a comparison across Hemiptera, we are able to confirm the hypothesis of Pal and Vicoso (2015) that the hemipteran X chromosome has substantial conservation of gene content.

Altogether, this study shows that long-read sequencing and chromosome-scale assemblies can uncover large-scale rearrangement events that are likely to have significantly impacted aphid genome evolution. We show that repeats are likely to play an important role in driving genome rearrangements in aphids. As such, aphids serve as an excellent model system to understand the role of genome rearrangements in species radiations and adaptation.

Materials and Methods

Aphid Genome Assembly Strategy

To assemble high-quality reference genomes for *M. persicae* and *A. pisum*, we generated initial de novo contig assemblies based on high-coverage Nanopore long-read data. These assemblies were then scaffolded into pseudomolecules (chromosomes) using in vivo chromatin conformation capture (HiC) data (Dudchenko et al. 2017) and, in the case of *A. pisum*, 10X Genomics Chromium linked reads (Zheng et al. 2016; Weisenfeld et al. 2017). As *M. persicae* and *A. pisum*

have divergent genome architectures (e.g., repeat content and level of heterozygosity), we optimized the initial contig assembly for each species, aiming to maximize genome completeness and minimize pseudo duplication caused by under-collapsed heterozygosity. These criteria were assessed by comparing the K-mer content of raw sequencing reads to the genome assembly with the K-mer Analysis Toolkit (Mapleson et al. 2017) and by assessing the representation of conserved genes with BUSCO v3 (Simão et al. 2015; Waterhouse et al. 2018), using the Arthropoda gene set ($n = 1,066$). We also used genome size estimates for *M. persicae* (409 Mb) and *A. pisum* (514 Mb) based on flow cytometry from Wenger et al. (2020) to assess the proportion of the genome that had been assembled and to estimate sequence read coverage. For each species, we compared long-read assemblies generated with Canu (Koren et al. 2017), Flye (Kolmogorov et al. 2019), and wtdbg2 (Ruan and Li 2019) as well as various combinations of assembly merging with quickmerge (Chakraborty et al. 2016), the effect of removing alternative haplotypes and the effect of long- and short-read assembly polishing (supplementary note, Supplementary Material online). Below, we describe the steps used to generate the final genome assembly for each species.

Sequencing and De Novo Assembly of *M. persicae* Clone O

We previously sequenced the genome of *M. persicae* clone O using Illumina short-read sequencing (Mathers et al. 2017). We used aphids derived from the same asexually reproducing colony maintained at the John Innes Centre insectary for all DNA extractions.

For Nanopore long-read sequencing, batches of 20 aphids were collected in 1.5-ml low-bind Eppendorf tubes and snap frozen in liquid nitrogen. We extracted high molecular weight DNA with the Illustra Nucleon PhytoPure kit (GE Healthcare, RPN8511) following the manufacturers protocol. Wide-bore pipette tips were used when transferring solutions to circumvent shearing of DNA. DNA concentration was determined using the Qubit broad-range assay. The purity of each extraction was assessed using a NanoDrop spectrophotometer (Thermo Fisher) based on 260/280 and 260/230 nm absorbance values, and by comparing the NanoDrop concentration estimate to the Qubit estimate, looking for a ratio close to 1:1 (Schalamun et al. 2019). The length of extracted DNA molecules was assessed using a Femto fragment analyzer (Agilent). Nanopore genomic DNA libraries were prepared for samples passing quality control using the Ligation Sequencing Kit (Oxford Nanopore Technologies [ONT], Oxford, UK: SQK-LSK109) following the manufacturers protocol with the exception that we started with 10 μ g of high molecular weight DNA. In total, four libraries were generated and each one sequenced on an R9.4 flow cell for 72 h. Base calling was run using Guppy v2.3.1 (ONT, Oxford, UK) with default settings, retaining reads with a quality score of at least 7. This resulted in a total of 28 Gb of data ($\sim 70\times$ coverage of the *M. persicae* genome) with a an N50 of 23 kb (supplementary table 7, Supplementary Material online).

We also generated 24 Gb ($\sim 59\times$ coverage) of Illumina short reads for assembly polishing and quality control. DNA was extracted from ~ 50 individuals with a modified CTAB protocol (Marzachi et al. 1998) and sent to Novogene (China) for sequencing. Novogene prepared a polymerase chain reaction-free Illumina sequencing library using the NEBNext Ultra II DNA Library Prep Kit for Illumina (New England Biolabs, USA), with the manufacturers protocol modified to give a 500-bp–1-kb insert size. This library was sequenced on an Illumina HiSeq 2500 instrument with 250-bp paired-end chemistry. The resulting reads were trimmed for adapter sequences with trim_galore! v0.4.0 (Krueger 2015), retaining read pairs where both sequences were at least 150-bp long after adapter trimming.

In our exploratory analysis, wtdgb2 v2.3 gave optimum performance for assembling the *M. persicae* clone O Nanopore data (supplementary note, Supplementary Material online). We generated two wtdgb2 assemblies with the parameters “-x ont -p 0 -k 17 -L 15000” and “-x ont -p 19 -k 0 -L 15000.” These assemblies had complementary contiguity and contained nonoverlapping sets of BUSCO genes. We therefore merged the two wtdgb2 genome assemblies with quickmerge v0.3 using the parameters “-l 1837291 -ml 10000,” with the more complete wtdgb2 “-x ont -p 0 -k 17 -L 15000” assembly used as the query. This resulted in an assembly that was more complete and more contiguous than either individual wtdgb2 assembly (see supplementary note, Supplementary Material online). The merged wtdgb2 assembly was then iteratively polished, first with three rounds of long-read polishing with racon v1.3.1 (Vaser et al. 2017), then with three rounds of short-read polishing with Pilon v1.22 (Walker et al. 2014) in diploid mode. Redundant haplotigs (contigs derived from uncollapsed heterozygosity) were removed from the polished assembly with Purge Haplotigs (Roach et al. 2018) using the sequence coverage bounds 9, 45, and 92, and requiring contigs to cover at least 90% of another, longer contig, to be flagged as a haplotig.

Sequencing and De Novo Assembly of *A. pisum* Clone JIC1

An isolate of *A. pisum* (dubbed JIC1) found on *Lathyrus odoratus* (sweet pea) was collected from Norwich in 2005 and subsequently reared at the JIC insectary under controlled conditions (Bedford I, personal communication). DNA extractions and Nanopore sequencing libraries were prepared as described above for *M. persicae* clone O. In total, two libraries were generated and each one sequenced on an R9.4 flow cell for 72 h. Base calling was run using Guppy v2.3.1 with the “flip-flop” model, retaining reads with a quality score of at least 7. This resulted in a total of 18 Gb of data ($\sim 35\times$ coverage of the *A. pisum* genome) with an N50 of 33 kb (supplementary table 7, Supplementary Material online).

To improve the Nanopore de novo assembly and generate accurate Illumina short reads for assembly polishing, we generated 10X Genomics Chromium linked-read data using DNA extracted as described above. High molecular weight DNA was sent to Novogene (China) for 10X Genomics Chromium library preparation following the manufacturers protocol and

sequencing was performed on an Illumina NovaSeq instrument. In total we generated 45 Gb of 150-bp paired-end reads ($\sim 88\times$ coverage of the *A. pisum* genome). The average molecule size of the library was 32 kb (supplementary table 7, Supplementary Material online).

De novo assembly with Flye v2.4 using default settings gave the best balance between contiguity, genome completeness, and absence of erroneously duplicated content (supplementary note, Supplementary Material online). The Flye assembly was polished as described above for *M. persicae*, with three rounds of racon followed by three rounds of Pilon. For Pilon polishing, we used the 10X reads after removing barcodes and primer sequence with process_10xReads.py (https://github.com/ucdavis-bioinformatics/proc10xG, last accessed March 25, 2020). Redundant haplotigs were removed from the polished Flye assembly with Purge Haplotigs (Roach et al. 2018) using the sequence coverage bounds 4, 21, and 57, and requiring contigs to cover at least 75% of another, longer contig, to be flagged as a haplotig. Finally, we iteratively scaffolded the deduplicated Flye assembly using our 10X Genomics linked-read data. We ran two iterations of Scaff10x v4.0 (https://github.com/wtsi-hpag/Scaff10x, last accessed March 25, 2020) with the parameters “-longread 1 -edge 45000 -block 45000” followed by Tigmint v1.1.2 (Jackman et al. 2018) with default settings, which identifies misassemblies, breaks the assembly, and performs a final round of scaffolding with ARCS (Yeo et al. 2018).

HiC Libraries and Genome Scaffolding

To scaffold our de novo assemblies of *M. persicae* clone O and *A. pisum* clone JIC1, we used in vivo chromatin conformation capture to generate HiC data. For each species, whole bodies of individuals from the same clonal populations used for genome sequencing were snap frozen in liquid nitrogen and sent to Dovetail Genomics (Santa Cruz, CA) for HiC library preparation and sequencing. HiC libraries were prepared using the *DpnII* restriction enzyme following a similar protocol to Lieberman-Aiden et al. (2009). HiC libraries were sequenced on an Illumina HiSeq X instrument, generating 150-bp paired-end reads. In total, we generated 123 Gb ($\sim 300\times$ coverage) and 21 Gb ($\sim 40\times$ coverage) of HiC data for *M. persicae* clone O and *A. pisum* clone JIC1, respectively (supplementary table 7, Supplementary Material online). To identify HiC contacts, we aligned our HiC data to our draft assemblies using the Juicer pipeline (Durand et al. 2016). We then used the 3D-DNA assembly pipeline (Dudchenko et al. 2017) to first correct misassemblies in each input assembly and then to order contigs (or scaffolds for *A. pisum* JIC1) into superscaffolds. K-mer analysis showed that our draft assemblies did not contain substantial quantities of duplicated content caused by the inclusion of haplotigs so we ran 3D-DNA in “haploid mode” with default settings for *M. persicae* clone O and “-editor-repeat-coverage 4” for *A. pisum* JIC1 (supplementary note, Supplementary Material online). The initial HiC assembly for each species was then manually reviewed using Juicebox Assembly Tools to correct misjoins and other errors (Dudchenko et al. 2018). Following Juicebox Assembly Tools review, the assemblies were polished with the 3D-DNA

seal module to reintegrate genomic content removed from superscaffolds by false positive manual edits to create a final scaffolded assembly. The HiC assemblies were then screened for contamination with BlobTools (Kumar et al. 2013; Laetsch and Blaxter 2017). Finally, a frozen release was generated for each assembly with scaffolds renamed and ordered by size with SeqKit v0.9.1 (Shen et al. 2016). The final assemblies were checked with BUSCO and K-mer Analysis Toolkit comp to ensure the scaffolding and decontamination steps had not reduced gene-level completeness or removed genuine single-copy aphid genome content.

Transcriptome Sequencing of *M. persicae* Morphs

We previously sequenced the transcriptomes *M. persicae* clone O apterous (unwinged) asexual females and alate (winged) males using six biological replicates per morph (Mathers et al. 2019). As part of the same experiment, we also collected and sequenced nymphs (derived from apterous asexual females) and alate asexual females (also six biological replicates each). These data were not used in our original study (Mathers et al. 2019) but are included here for genome annotation and to provide a more comprehensive view of morph-biased gene expression in *M. persicae*. Aphid rearing, RNA extraction, and sequencing were carried out as in Mathers et al. (2019). Apterous asexual females, alate asexual females, and nymphs were reared in long day conditions (14 h light, 22 °C day time, and 20 °C night time, 48% relative humidity) and alate males were reared in short day conditions (8 h light, 18 °C day time, and 16 °C night time, 48% relative humidity).

Genome Annotation

We annotated protein-coding genes in our new chromosome-level assemblies of *M. persicae* and *A. pisum* using BRAKER2 v2.1.2 (Hoff et al. 2016, 2019), incorporating evidence from RNA-seq alignments. Prior to running BRAKER2, we soft-masked each genome with RepeatMasker v4.0.7 (Tarailo-Graovac and Chen 2009; Smit et al. 2015) using known Insecta repeats from Repbase (Bao et al. 2015) with the parameters “-e ncbi -species insecta -a xsmall -gff.” We then aligned RNA-seq data to the soft-masked genomes with HISAT2 v2.0.5 (Kim et al. 2015). All RNA-seq data sets used for annotation are summarized in supplementary table 8, Supplementary Material online. For *M. persicae*, we aligned 25 RNA-seq libraries. Specifically, we used a high-coverage (~200 million reads), strand-specific, RNA-seq library generated from mixed whole bodies of apterous *M. persicae* clone O asexual females (Mathers et al. 2017) as well as newly generated (see above) and publicly available (Mathers et al. 2019) unstranded RNA-seq data for *M. persicae* clone O nymphs (derived from apterous asexual females), alate asexual females, apterous asexual females and males (six biological replicates each). All RNA-seq data were trimmed for adapters and low quality bases (quality score < 20) with Trim Galore v0.4.5 (Krueger 2015), retaining reads where both members of the pair are at least 20-bp long. Unstranded RNA-seq data were aligned to the genome with HISAT2 with the parameters “-max-intronlen 25000 -dta-

cufflinks” followed by sorting and indexing with SAMtools v1.3 (Li et al. 2009). Strand-specific RNA-seq was mapped as for the unstranded data, with the addition of the HISAT2 parameter “-rna-strandness RF.” We then ran BRAKER2 with UTR training and prediction enabled with the parameters “-softmasking -gff3 -UTR=on.” Strand-specific RNA-seq alignments were split by forward and reverse strands and passed to BRAKER2 as separate BAM files to improve the accuracy of UTR models as recommended in the BRAKER2 documentation. For *A. pisum* clone JIC1, we used unstranded RNA-seq data derived from whole bodies of *A. pisum* clone LSR1 (IAGC 2010) males, asexual females, and sexual females (two biological replicates each) from Jaquière et al. (2013). Reads were, trimmed, mapped, and passed to BRAKER2 as for the unstranded *M. persicae* RNA-seq data. Following gene prediction, genes were removed that contained in frame stop codons using the BRAKER2 script getAnnoFastaFromJoiningenes.py and the completeness of each gene set was checked with BUSCO using the longest transcript of each gene as the representative transcript.

X Chromosome Identification

We identified the aphid sex (X) chromosome in our new assemblies of *M. persicae* clone O and *A. pisum* JIC1 based on the ratio of male (M) to asexual female (FA) coverage of Illumina genomic DNA reads. For *M. persicae*, we used whole-genome bisulfite sequencing (BS-seq) reads from Mathers et al. (2019), merging biological replicates by morph. These data are derived from the same clonal population (clone O) as used for the genome assembly. BS-seq reads were aligned to the *M. persicae* clone O v2 genome with Bismark v0.20.0 (Krueger and Andrews 2011) with default parameters. We used Sambamba v0.6.8 to estimate BS-seq read depth in 100-kb fixed windows for M and FA separately using the BAM files generated by Bismark and the parameters “depth window -fix-mate-overlaps -window-size = 100000 -overlap = 100000.” We then calculated the ratio of M to FA read depth per window (i.e., the coverage ratio). Coverage ratios showed scaffold 1 to have the expected X chromosome M to FA coverage ratio (50% that of the autosomes). To generate figure 1c, we calculated average M (107×) and FA (82×) coverage excluding scaffold 1 to derive a coverage correction factor for FA (×1.3) and used this to calculate normalized M to FA coverage ratio for each 100 kb window. For *A. pisum* JIC1, we used whole-genome Illumina sequence data of clone AL4 M and FA morphs from Li et al. (2019). We followed the same procedure as for *M. persicae* clone O with the exception of using BWA-MEM v0.7.17 (Li 2013) to map reads and Sambamba markdup to identify reads derived from polymerase chain reaction duplicates prior to calculating coverage statistics. Scaffold 1 was identified as the X chromosome. Excluding scaffold 1, we calculated average M (45×) and FA (41×) coverage to derive a coverage correction factor for FA (×1.1) and used this to calculate normalized M to FA coverage ratio for each 100-kb window along *A. pisum* JIC1 chromosome-length scaffolds to generate figure 1d.

Reannotation of the Chromosome-Scale Assemblies of *Rhod. prolixus* and *T. rubrofasciata*

We included the recently released chromosome-scale genome assemblies of the blood-feeding hemipterans *Rhod. prolixus* (obtained from the DNA Zoo [https://www.dnazoo.org/, last accessed March 25, 2020; Dudchenko et al. 2017]) and *T. rubrofasciata* (Liu et al. 2019) in our synteny and phylogenomic analyses. The *Rhod. prolixus* chromosome-level assembly has not yet been annotated and we found on initial inspection that the *T. rubrofasciata* gene release is based on the contig assembly of this species and not the chromosome-length scaffolds. We therefore generated de novo gene predictions for these two species using BRAKER2 with evidence from protein alignments created with GenomeThreader v1.7.1 (Gremme et al. 2005). For each species, we soft-masked the genome for known repeats as for *M. persicae* and *A. pisum*. We then ran BRAKER2 with the parameters “-softmasking -gff3 -prg=gth -trainFromGth.” For *Rhod. prolixus*, we used proteins from the original gene release as evidence (Mesquita et al. 2015). For *T. rubrofasciata*, we used proteins from Liu et al. (2019). The final BRAKER2 gene sets for each species were checked completeness using BUSCO as for *M. persicae* and *A. pisum*.

Phylogenomic Analysis of Sequenced Hemipteran Genomes

We estimated a time calibrated phylogeny of Hemiptera using protein sequences from our new genome assemblies of *M. persicae* clone O and *A. pisum* clone JIC1, the new annotations of the chromosome-scale assemblies of *Rhod. prolixus* and *T. rubrofasciata* and ten previously sequenced Hemiptera: *Myzus cerasi* (Thorpe et al. 2018), *Diuraphis noxia* (Nicholson et al. 2015), *Pentalonia nigronervosa* (Mathers et al. 2020a), *R. maidis* (Chen et al. 2019), *Rhopalosiphum padi* (Thorpe et al. 2018), *Aphis glycines* (version 2) (Mathers 2020), *Bemisia tabaci* MEAM1 (Chen et al. 2016), *Oncopeltus fasciatus* (Panfilio et al. 2019), *Sogatella furcifera* (Wang et al. 2017), and *Nilaparvata lugens* (Xue et al. 2014). Where multiple transcripts of a gene were annotated, we used the longest transcript to represent the gene model. We used OrthoFinder v2.2.3 (Emms and Kelly 2015, 2019) with Diamond v0.9.14 (Buchfink et al. 2015), MAFFT v7.305 (Katoh and Standley 2013), and FastTree v2.1.7 (Price et al. 2009, 2010) to cluster proteins into orthogroups, reconstruct gene trees, and estimate the species tree. The OrthoFinder species tree was rooted according to Johnson et al. (2018). To estimate approximate divergence times for our taxa of interest, we used penalized likelihood implemented in r8s with secondary calibration points derived from Johnson et al. (2018) (supplementary table 9, Supplementary Material online).

Synteny Analysis

We identified syntenic blocks of genes between *M. persicae*, *A. pisum*, and *R. maidis*, and between *Rhod. prolixus* and *T. rubrofasciata*, using MCScanX v1.1 (Wang et al. 2012). For each comparison, we carried out an all versus all BLAST search of annotated protein sequences using BLASTALL v2.2.22 (Altschul et al. 1990) with the options “-p BlastP - e

1e-10 -b 5 -v 5 -m 8” and ran MCScanX with the parameters “-s10 -b 2,” requiring synteny blocks to contain at least ten consecutive genes and to have a gap of no more than 25 genes. MCScanX results were visualized with SynVisio (https://synvisio.github.io/#/, last accessed March 25, 2020). We parsed the MCScanX results and estimated synonymous and nonsynonymous substitution rates between pairs of syntenic genes using collinearity scripts from Nowell et al. (2018; https://github.com/reubwn/collinearity, last accessed March 25, 2020). We also investigated synteny using orthologous genes identified by OrthoFinder. We performed two additional OrthoFinder runs, one with the chromosome-scale assemblies of *M. persicae*, *A. pisum*, and *R. maidis*, and one using the three aphid assemblies and the chromosome-scale assembly of *Rhod. prolixus*. OrthoFinder was run as described above for the phylogenomic analysis of Hemiptera.

To test for conservation of the X chromosome across Hemiptera, we first identified *Rhod. prolixus* chromosomes that were likely to be homologous to *M. persicae* chromosomes. We therefore mapped their orthologous genes onto chromosomes. Next, we tested for significant enrichment of genes from specific *Rhod. prolixus* (target) chromosomes on each *M. persicae* (focal) chromosome using a binomial test. In each binomial test, the observed ortholog count from a target *Rhod. prolixus* chromosome is the *number of successful trials*. The total number of orthologs on the *M. persicae* focal chromosome is the *total number of trials* (this is equal to the sum of all *Rhod. prolixus* orthologs that map to the focal chromosome). Finally, the *probability of success* is equal to the fraction of orthologs found on the *Rhod. prolixus* target chromosome, relative to the total number of orthologs. We corrected for multiple testing using the BH procedure (Benjamini and Hochberg 1995). For each focal *M. persicae* chromosome, we also calculated the observed/expected ratio of orthologs from each target *Rhod. prolixus* chromosome. The expected ortholog count was calculated by multiplying the total ortholog count for the focal *M. persicae* chromosome by the fraction of all *M. persicae*-*Rhod. prolixus* orthologs found on the target *Rhod. prolixus* chromosome.

Myzus persicae Gene Expression

We investigated patterns of gene expression in the *M. persicae* clone O v2 genome using newly generated (see above) and previously published (Mathers et al. 2019) RNA-seq data for *M. persicae* clone O nymphs (derived from unwinged asexual females), winged asexual females, unwinged asexual females, and winged males (six biological replicates each). Transcript-level expression was estimated for each sample with Kallisto v0.44.0 (Bray et al. 2016) with 100 bootstrap replicates. We identified differentially expressed genes between *M. persicae* morphs using Sleuth (Pimentel et al. 2017), aggregating transcript-level *P* values (Yi et al. 2018). Specifically, we used a likelihood ratio test to identify genes that significantly vary by morph (BH corrected $P < 0.05$). To quantify the magnitude of the change in expression relative to unwinged asexual females (from which the other morphs are derived), we applied pairwise Wald tests between unwinged asexual females and each alternative morph and recorded the effect size

(beta) which approximates the \log_2 fold change in expression. We considered genes to be “morph biased” if they had a significant likelihood ratio test result and $\text{abs. beta} > 0.5$ in any morph relative to unwinged asexual females. To identify genes that were specifically upregulated in males, we identified the subset of “morph-biased” genes that had $\text{beta} > 0.5$ in winged males and $\text{beta} < 0.5$ in winged asexual females and nymphs.

To test for dosage compensation in *M. persicae* clone O, we calculated the \log_2 ratio of winged male to unwinged asexual female gene expression using transcripts per million (TPM) expression values estimated by Kallisto for all genes with expression of at least one TPM in both morphs. For each gene, we used the longest transcript to represent the gene. We then compared expression ratios for genes on the X chromosome and the autosomes with a Wilcoxon rank-sum test.

TE Analysis

To investigate the distribution of TEs in *M. persicae* clone O v2 and *A. pisum* JIC1 v1, we generated a comprehensive TE annotation. For each assembly, we modeled TEs de novo with RepeatModeler v1.0.8 (Smit and Hubley 2008) and then merged the de novo repeats with known repeats from the RepBase Insecta library (Bao et al. 2015) using ReannTE_MergeFasta.pl (<https://github.com/4ureliek/ReannTE>). We then annotated TEs across each genome with RepeatMasker v4.0.7 (Smit et al. 2005; Tarailo-Graovac and Chen 2009) using the species-specific merged TE library. We calculated TE density in 100 kb and 1 Mb fixed windows with DensityMap (Guizard et al. 2016), grouping all TEs together, and also separately for DNA transposons, LINEs, LTR retrotransposons, rolling-circle transposons, and short interspersed nuclear elements. We also calculated the density of expressed genes in the same windows. For *M. persicae*, we used genes classified as expressed by sleuth (estimated count > 4 in at least 12/24 samples) in the “morph-biased” expression analysis (above). To generate equivalent data for *A. pisum*, we ran Kallisto and Sleuth as for the *M. persicae* morph-biased expression analysis (above) using RNA-seq data derived from whole bodies of *A. pisum* clone LSR1 (IAGC 2010) males, asexual females, and sexual females (two biological replicates each) from Jaquiéry et al. (2013). Genes were considered expressed if they had an estimated read count > 4 in at least three out of six samples.

We investigated the repeat content of autosomal synteny blocks and autosomal synteny breakpoint regions in *M. persicae* clone O v2 and *A. pisum* JIC1 v1 using BEDTools v2.28.0 (Quinlan and Hall 2010) and the TE annotations described above. We defined synteny breakpoint regions as the gaps between synteny blocks identified by MCScanX analysis of *M. persicae* clone O v2 and *A. pisum* JIC1 v1 (see Synteny Analysis). The genomic coordinates of synteny blocks were defined based on the start position of the first gene and the end position of the last gene in each block. We then identified the genomic coordinates of synteny breakpoint regions using BEDTools complement (i.e., we identified all regions in between autosomal synteny blocks). We excluded chromosome ends as they may or may not

correspond to breakpoint regions and may contain repetitive (sub)telomeric sequence that would bias our analysis (i.e., breakpoint regions had to be flanked by a synteny block at either end). As synteny blocks were defined based on the locations of homologous genes (rather than sequence alignments) and allow gaps of up to 25 genes within blocks, our analysis should not be affected by the breakup of synteny blocks by lineage-specific TE accumulation within otherwise syntenic genomic regions. TEs overlapping synteny blocks and breakpoint regions were identified using BEDTools intersect and we recorded the span (in bp) and count of TEs by class (i.e., summing independently for DNA, LINE, LTR, rolling-circle, SINE, and unclassified TEs). To test for significant enrichment of TEs within synteny breakpoint regions, we simulated 10,000 sets of random regions, each with the same size distribution as the observed synteny breakpoint regions, and repeated the analysis. *P* values for each TE class were determined based on the number of simulated regions with a TE count equal to or greater than the TE count of the same class in the observed synteny breakpoint regions divided by the number of simulations ($n = 10,000$). Additionally, for each TE class, we calculated the expected span in bp within autosomal synteny breakpoint regions based on the total size of the autosomal synteny breakpoint regions and the autosomal TE proportion of each class and compared this with the observed value. These analysis were carried out independently using both *M. persicae* clone O v2 and *A. pisum* JIC1 v1 as the reference.

To generate TE age distributions for *M. persicae* clone O v2 and *A. pisum* JIC1, we ran RepeatMasker separately for the autosomes and the X chromosome for each species and parsed the output with parseRM_GetLandscape.pl (<https://github.com/4ureliek/Parsing-RepeatMasker-Outputs>, last accessed March 25, 2020). We used the CpG adjusted Kimura 2-parameter distance of each TE insertion from its corresponding consensus sequence as a proxy for TE age.

Supplementary Material

Supplementary data are available at *Molecular Biology and Evolution* online.

Acknowledgments

This work was funded by a Biotechnology and Biological Sciences Research Council (BBSRC) Future Leader Fellowship (BB/R01227X/1) awarded to T.C.M. and the BBSRC Industrial Partnership Awards (IPAs) with Syngenta Ltd (BB/L002108/1 and BB/R009481/1) awarded to S.A.H., D.S. and C.V.O. R.H.M.W. was funded from the BBSRC Norwich Research Park Biosciences Doctoral Training Partnership Award (BB/M011216/1). Additional support was received from the BBSRC Institute Strategy Programme (BB/P012574/1) and the John Innes Foundation. This research was supported in part by the NBI Computing Infrastructure for Science Group, which provides technical support and maintenance to the John Innes Centre’s high-performance computing cluster and storage systems. We thank the JIC Entomology Facility for assistance with rearing of aphids

and in particular Dr Ian Bedford for collecting the isolate of *Acyrtosiphon pisum* dubbed JIC1 and Anna Jordan for identification of *Myzus persicae* morphs.

Data Availability

Raw sequence data generated for this study are available at the NCBI short-read archive under BioProject PRJNA613055. Genome assemblies, annotations, and [supplementary data](#) are available from Zenodo: <https://zenodo.org/record/3712089#.Xz7WERPdvRZ>. Genome assemblies and annotations of *M. persicae* clone O v2 and *A. pisum* JIC1 v1 can also be found at AphidBase (<https://bipaa.genouest.org/is/aphidbase/>).

References

- Ahola V, Lehtonen R, Somervuo P, Salmela L, Koskinen P, Rastas P, Välimäki N, Paulin L, Kvist J, Wahlberg N, et al. 2014. The Glanville fritillary genome retains an ancient karyotype and reveals selective chromosomal fusions in Lepidoptera. *Nat Commun.* 5:4737.
- Altschul SF, Gish W, Miller W, Myers EW, Lipman DJ. 1990. Basic local alignment search tool. *J Mol Biol.* 215(3):403–410.
- Bao W, Kojima KK, Kohany O. 2015. Repbase Update, a database of repetitive elements in eukaryotic genomes. *Mob DNA* 6:4–9.
- Benjamini Y, Hochberg Y. 1995. Controlling the false discovery rate: a practical and powerful approach to multiple testing. *J R Stat Soc B.* 57(1):289–300.
- Blackman RL. 1971. Chromosomal abnormalities in an anholocyclic biotype of *Myzus persicae* (Sulzer). *Experientia* 27(6):704–706.
- Blackman R. 1980. Chromosome numbers in the Aphididae and their taxonomic significance. *Syst Entomol.* 5(1):7–25.
- Blackman RL, Spence JM, Normark BB. 2000. High diversity of structurally heterozygous karyotypes and rDNA arrays in parthenogenetic aphids of the genus *Trama* (Aphididae: Lachninae). *Heredity (Edinb).* 84(2):254–260.
- Blackmon H, Ross L, Bachtrog D. 2017. Sex determination, sex chromosomes, and karyotype evolution in insects. *J Hered.* 108(1):78–93.
- Bracewell R, Chatla K, Nalley MJ, Bachtrog D. 2019. Dynamic turnover of centromeres drives karyotype evolution in *Drosophila*. *Elife* 8:e49002.
- Bracewell R, Tran A, Chatla K, Bachtrog D. 2020. Chromosome-level assembly of *Drosophila bifasciata* reveals important karyotypic transition of the X chromosome. *G3 (Bethesda)* 10:891–897.
- Bray NL, Pimentel H, Melsted P, Pachter L. 2016. Near-optimal probabilistic RNA-seq quantification. *Nat Biotechnol.* 34(5):525–527.
- Brisson JA, Stern DL. 2006. The pea aphid, *Acyrtosiphon pisum*: an emerging genomic model system for ecological, developmental and evolutionary studies. *BioEssays* 28(7):747–755.
- Buchfink B, Xie C, Huson DH. 2015. Fast and sensitive protein alignment using DIAMOND. *Nat Methods.* 12(1):59–60.
- Chakraborty M, Baldwin-Brown JG, Long AD, Emerson JJ. 2016. Contiguous and accurate de novo assembly of metazoan genomes with modest long read coverage. *Nucleic Acids Res.* 44:1–12.
- Chakraborty M, VanKuren NW, Zhao R, Zhang X, Kalsow S, Emerson JJ. 2018. Extensive hidden genetic variation shapes the structure of functional elements in *Drosophila*. *Nat Genet.* 50(1):20–25.
- Chang SL, Lai HY, Tung SY, Leu JY. 2013. Dynamic large-scale chromosomal rearrangements fuel rapid adaptation in yeast populations. *PLoS Genet.* 9(1):e1003232.
- Charlesworth B. 2009. Fundamental concepts in genetics: effective population size and patterns of molecular evolution and variation. *Nat Rev Genet.* 10(3):195–205.
- Charlesworth B, Charlesworth D. 2017. Population genetics from 1966 to 2016. *Heredity (Edinb).* 118(1):2–9.
- Chen W, Hasegawa DK, Kaur N, Kliot A, Pinheiro PV, Luan J, Stensmyr MC, Zheng Y, Liu W, Sun H, et al. 2016. The draft genome of whitefly *Bemisia tabaci* MEAM1, a global crop pest, provides novel insights into virus transmission, host adaptation, and insecticide resistance. *BMC Biol.* 14(1):110.
- Chen W, Shakir S, Bigham M, Richter A, Fei Z, Jander G. 2019. Genome sequence of the corn leaf aphid (*Rhopalosiphum maidis* Fitch). *Gigascience* 8(4):1–12.
- Chénais B, Caruso A, Hiard S, Casse N. 2012. The impact of transposable elements on eukaryotic genomes: from genome size increase to genetic adaptation to stressful environments. *Gene* 509(1):7–15.
- d’Alençon E, Sezutsu H, Legeai F, Permal E, Bernard-Samain S, Gimenez S, Gagneur C, Cousserans F, Shimomura M, Brun-Barale A, et al. 2010. Extensive synteny conservation of holocentric chromosomes in Lepidoptera despite high rates of local genome rearrangements. *Proc Natl Acad Sci U S A.* 107(17):7680–7685.
- Davey J, Chouteau M, Barker SL, Maroja L, Baxter SW, Simpson F, Merrill RM, Joron M, Mallet J, Dasmahapatra KK, et al. 2015. Major improvements to the *Heliconius melpomene* genome assembly used to confirm 10 chromosome fusion events in 6 million years of butterfly evolution. *G3 (Bethesda)* 6:695–708.
- Denton JF, Lugo-Martinez J, Tucker AE, Schrider DR, Warren WC, Hahn MW. 2014. Extensive error in the number of genes inferred from draft genome assemblies. *PLoS Comput Biol.* 10(12):e1003998.
- Dixon AFG. 1977. Aphid ecology: life cycles, polymorphism, and population regulation. *Annu Rev Ecol Syst.* 8(1):329–353.
- Drinnenberg IA, DeYoung D, Henikoff S, Malik HS. 2014. Recurrent loss of CenH3 is associated with independent transitions to holocentricity in insects. *Elife* 3:e03676.
- Dudchenko O, Batra SS, Omer AD, Nyquist SK, Hoeger M, Durand NC, Shamim MS, Machol I, Lander ES, Aiden AP, et al. 2017. De novo assembly of the *Aedes aegypti* genome using Hi-C yields chromosome-length scaffolds. *Science* 356(6333):92–95.
- Dudchenko O, Shamim MS, Batra S, Durand NC, Musial NT, Mostofa R, Pham M, St Hilaire BG, Yao W, Stamenova E, et al. 2018. The Juicebox Assembly Tools module facilitates de novo assembly of mammalian genomes with chromosome-length scaffolds for under \$1000. *bioRxiv* 254797.
- Durand NC, Shamim MS, Machol I, Rao SSP, Huntley MH, Lander ES, Aiden EL. 2016. Juicer provides a one-click system for analyzing loop-resolution Hi-C experiments. *Cell Syst.* 3(1):95–98.
- Eichler EE, Sankoff D. 2003. Structural dynamics of eukaryotic chromosome evolution. *Science* 301(5634):793–797.
- Emms DM, Kelly S. 2015. OrthoFinder: solving fundamental biases in whole genome comparisons dramatically improves orthogroup inference accuracy. *Genome Biol.* 16(1):157.
- Emms DM, Kelly S. 2019. OrthoFinder: phylogenetic orthology inference for comparative genomics. *Genome Biol.* 20(1):14.
- Farré M, Kim J, Proskuryakova AA, Zhang Y, Kulemzina AI, Li Q, Zhou Y, Xiong Y, Johnson JL, Perelman PL, et al. 2019. Evolution of gene regulation in ruminants differs between evolutionary breakpoint regions and homologous synteny blocks. *Genome Res.* 29(4):576–589.
- Farré M, Micheletti D, Ruiz-Herrera A. 2013. Recombination rates and genomic shuffling in human and chimpanzee—a new twist in the chromosomal speciation theory. *Mol Biol Evol.* 30(4):853–864.
- Fernández R, Marcet-Houben M, Legeai F, Richard G, Robin S, Wucher V, Pegueroles C, Gabaldón T, Tagu D. 2020. Selection following gene duplication shapes recent genome evolution in the pea aphid *Acyrtosiphon pisum*. *Mol Biol Evol.* 37(9):2601–2615.
- Fuller ZL, Koury SA, Phadnis N, Schaeffer SW. 2019. How chromosomal rearrangements shape adaptation and speciation: case studies in *Drosophila pseudoobscura* and its sibling species *Drosophila persimilis*. *Mol Ecol.* 28(6):1283–1301.
- Good BH, McDonald MJ, Barrick JE, Lenski RE, Desai MM. 2017. The dynamics of molecular evolution over 60,000 generations. *Nature* 551(7678):45–50.
- Gremme G, Brendel V, Sparks ME, Kurtz S. 2005. Engineering a software tool for gene structure prediction in higher organisms. *Inf Softw Technol.* 47(15):965–978.
- Guerrero RF, Kirkpatrick M. 2014. Local adaptation and the evolution of chromosome fusions. *Evolution (N Y).* 68(10):2747–2756.

- Guizard S, Piégu B, Bigot Y. 2016. DensityMap: a genome viewer for illustrating the densities of features. *BMC Bioinf.* 17(1):6.
- Hawthorne DJ, Via S. 2001. Genetic linkage of ecological specialization and reproductive isolation in pea aphids. *Nature* 412(6850):904–931.
- Heliconius Genome Consortium, Dasmahapatra KK, Walters JR, Briscoe AD, Davey JW, Whibley A, Nadeau NJ, Zimin AV, Hughes DST, Ferguson LC, et al. 2012. Butterfly genome reveals promiscuous exchange of mimicry adaptations among species. *Nature* 487:94–98.
- Hill J, Rastas P, Hornett EA, Neethiraj R, Clark N, Morehouse N, de la Paz Celorio-Mancera M, Cols JC, Dirksen H, Meslin C, et al. 2019. Unprecedented reorganization of holocentric chromosomes provides insights into the enigma of lepidopteran chromosome evolution. *Sci Adv.* 5(6):eaau3648.
- Hoff KJ, Lange S, Lomsadze A, Borodovsky M, Stanke M. 2016. BRAKER1: unsupervised RNA-Seq-based genome annotation with GeneMark-ET and AUGUSTUS. *Bioinformatics* 32(5):767–769.
- Hoff KJ, Lomsadze A, Borodovsky M, Stanke M. 2019. Whole-genome annotation with BRAKER. In: Kollmar M, editor. *Gene prediction: methods and protocols*. New York: Springer. p. 65–95.
- Hughes-Schrader S, Schrader F. 1961. The kinetochore of the Hemiptera. *Chromosoma* 12(1):327–350.
- IAGC. 2010. Genome sequence of the pea aphid *Acyrtosiphon pisum*. *PLoS Biol.* 8:e1000313.
- Jackman SD, Coombe L, Chu J, Warren RL, Vandervalk BP, Yeo S, Xue Z, Mohamadi H, Bohlmann J, Jones SJM, et al. 2018. Tigmint: correcting assembly errors using linked reads from large molecules. *BMC Bioinf.* 19(1):393.
- Jaquière J, Peccoud J, Ouisse T, Legeai F, Prunier-Leterme N, Gouin A, Nouhaud P, Brisson JA, Bickel R, Purandare S, et al. 2018. Disentangling the causes for faster-X evolution in aphids. *Genome Biol Evol.* 10(2):507–520.
- Jaquière J, Risper C, Roze D, Legeai F, Le Trionnaire G, Stoeckel S, Mieuze L, Da Silva C, Poulain J, Prunier-Leterme N, et al. 2013. Masculinization of the X chromosome in the pea aphid. *PLoS Genet.* 9(8):e1003690.
- Jaquière J, Stoeckel S, Larose C, Nouhaud P, Risper C, Mieuze L, Bonhomme J, Mahéo F, Legeai F, Gauthier J-P, et al. 2014. Genetic control of contagious asexuality in the pea aphid. *PLoS Genet.* 10(12):e1004838.
- Jaquière J, Stoeckel S, Risper C, Mieuze L, Legeai F, Simon J-C. 2012. Accelerated evolution of sex chromosomes in aphids, an X0 system. *Mol Biol Evol.* 29(2):837–847.
- Johnson KP, Dietrich CH, Friedrich F, Beutel RG, Wipfler B, Peters RS, Allen JM, Petersen M, Donath A, Walden KKO, et al. 2018. Phylogenomics and the evolution of hemipteroid insects. *Proc Natl Acad Sci U S A.* 115(50):12775–12780.
- Julca I, Marcet-Houben M, Cruz F, Vargas-Chavez C, Johnston JS, Gómez-Garrido J, Frias L, Corvelo A, Loska D, Cámara F, et al. 2020. Phylogenomics identifies an ancestral burst of gene duplications predating the diversification of Aphidomorpha. *Mol Biol Evol.* 37(3):730–756.
- Katoh K, Standley DM. 2013. MAFFT multiple sequence alignment software version 7: improvements in performance and usability. *Mol Biol Evol.* 30(4):772–780.
- Kim D, Langmead B, Salzberg SL. 2015. HISAT: a fast spliced aligner with low memory requirements. *Nat Methods.* 12(4):357–360.
- Kirkpatrick M, Barton N. 2006. Chromosome inversions, local adaptation and speciation. *Genetics* 173(1):419–434.
- Kolmogorov M, Yuan J, Lin Y, Pezner PA. 2019. Assembly of long, error-prone reads using repeat graphs. *Nat Biotechnol.* 37(5):540–546.
- Koren S, Walenz BP, Berlin K, Miller JR, Bergman NH, Phillippy AM. 2017. Canu: scalable and accurate long-read assembly via adaptive k -mer weighting and repeat separation. *Genome Res.* 27(5):722–736.
- Kronenberg ZN, Fiddes IT, Gordon D, Murali S, Cantsilieris S, Meyerson OS, Underwood JG, Nelson BJ, Chaisson MJP, Dougherty ML, et al. 2018. High-resolution comparative analysis of great ape genomes. *Science* 360(6393):eaar6343.
- Krueger F. 2015. Trim Galore. A wrapper tool around Cutadapt and FastQC to consistently apply quality and adapter trimming to FastQ files. Cambridge, UK: Babraham Institute.
- Krueger F, Andrews SR. 2011. Bismark: a flexible aligner and methylation caller for Bisulfite-Seq applications. *Bioinformatics* 27(11):1571–1572.
- Kumar S, Jones M, Koutsovoulos G, Clarke M, Blaxter M. 2013. Blobology: exploring raw genome data for contaminants, symbionts, and parasites using taxon-annotated GC-coverage plots. *Front Genet.* 4:1–12.
- Laetsch DR, Blaxter ML. 2017. BlobTools: interrogation of genome assemblies. *F1000Research* 6:1287.
- Li H. 2013. Aligning sequence reads, clone sequences and assembly contigs with BWA-MEM. arXiv arXiv:1303.3997v2.
- Li H, Handsaker B, Wysoker A, Fennell T, Ruan J, Homer N, Marth G, Abecasis G, Durbin R; 1000 Genome Project Data Processing Subgroup. 2009. The sequence alignment/map format and SAMtools. *Bioinformatics* 25(16):2078–2079.
- Li Y, Park H, Smith TE, Moran NA. 2019. Gene family evolution in the pea aphid based on chromosome-level genome assembly. *Mol Biol Evol.* 36(10):2143–2156.
- Li Y, Zhang B, Moran NA. 2020. The aphid X chromosome is a dangerous place for functionally important genes: diverse evolution of hemipteran genomes based on chromosome-level assemblies. *Mol Biol Evol.* 37(8):2357–2368.
- Lieberman-Aiden E, van Berkum NL, Williams L, Imakaev M, Ragozcy T, Telling A, Amit I, Lajoie BR, Sabo PJ, Dorschner MO, et al. 2009. Comprehensive mapping of long-range interactions reveals folding principles of the human genome. *Science* 326(5950):289–294.
- Liu Q, Guo Y, Zhang Y, Hu W, Li Y, Zhu D, Zhou Z, Wu J, Chen N, Zhou X-N. 2019. A chromosomal-level genome assembly for the insect vector for Chagas disease, *Triatoma rubrofasciata*. *Gigascience* 8:1–8.
- Lynch M, Ackerman MS, Gout J-F, Long H, Sung W, Thomas WK, Foster PL. 2016. Genetic drift, selection and the evolution of the mutation rate. *Nat Rev Genet.* 17(11):704–714.
- Mandrioli M, Zanasi F, Manicardi GC. 2014. Karyotype rearrangements and telomere analysis in *Myzus persicae* (Hemiptera, Aphididae) strains collected on *Lavandula* sp. plants. *Comp Cytogenet.* 8(4):259–274.
- Manicardi GC, Mandrioli M, Blackman RL. 2015. The cytogenetic architecture of the aphid genome. *Biol Rev Camb Philos Soc.* 90(1):112–125.
- Manicardi GC, Nardelli A, Mandrioli M. 2015. Fast chromosomal evolution and karyotype instability: recurrent chromosomal rearrangements in the peach potato aphid *Myzus persicae* (Hemiptera: Aphididae). *Biol J Linn Soc.* 116(3):519–529.
- Mank JE, Vicoso B, Berlin S, Charlesworth B. 2010. Effective population size and the Faster-X effect: empirical results and their interpretation. *Evolution (N Y).* 64(3):663–674.
- Manna GK. 1950. Multiple sex chromosome mechanism in a reduviid bug, *Conorhinus rubrofasciatus* (de Geer). *Proc Zool Soc (Bengal).* 3:155–161.
- Mapleson D, Accinelli GC, Kettleborough G, Wright J, Clavijo BJ. 2017. KAT: a K-mer Analysis Toolkit to quality control NGS datasets and genome assemblies. *Bioinformatics* 33(4):574–576.
- Martin SH, Davey JW, Salazar C, Jiggins CD. 2019. Recombination rate variation shapes barriers to introgression across butterfly genomes. *PLoS Biol.* 17(2):e2006288.
- Marzachi C, Veratti F, Bosco D. 1998. Direct PCR detection of phytoplasmas in experimentally infected insects. *Ann Appl Biol.* 133(1):45–54.
- Mathers TC. 2020. Improved genome assembly and annotation of the soybean aphid (*Aphis glycines* Matsumura). *G3 (Bethesda)* 10:899–906.
- Mathers TC, Chen Y, Kaithakottil G, Legeai F, Mugford ST, Baa-Puyoulet P, Bretaudeau A, Clavijo B, Colella S, Collin O, et al. 2017. Rapid transcriptional plasticity of duplicated gene clusters enables a clonally reproducing aphid to colonise diverse plant species. *Genome Biol.* 18(1):27.
- Mathers TC, Mugford ST, Percival-Alwyn L, Chen Y, Kaithakottil G, Swarbreck D, Hogenhout SA, Oosterhout C. 2019. Sex-specific changes in the aphid DNA methylation landscape. *Mol Ecol.* 28(18):4228–4241.
- Mathers TC, Mugford ST, Hogenhout SA, Tripathi L. 2020a. Genome Sequence of the Banana Aphid, *Pentalonia nigronervosa* Coquerel

- (Hemiptera: Aphididae) and Its Symbionts. *G3 (Bethesda)*. g3.401358.2020. doi: 10.1534/g3.120.401358.
- Mathers TC, Wouters RHM, Mugford ST, Swarbreck D, van Oosterhout C, Hogenhout SA. 2020b. Chromosome-scale genome assemblies of aphids reveal extensively rearranged autosomes and long-term conservation of the X chromosome. *bioRxiv* 2020.03.24.006411.
- Melters DP, Paliulis LV, Korf IF, Chan SWL. 2012. Holocentric chromosomes: convergent evolution, meiotic adaptations, and genomic analysis. *Chromosome Res.* 20(5):579–593.
- Mesquita RD, Vionette-Amaral RJ, Lowenberger C, Rivera-Pomar R, Monteiro FA, Minx P, Spieth J, Carvalho AB, Panzera F, Lawson D, et al. 2015. Genome of *Rhodnius prolixus*, an insect vector of Chagas disease, reveals unique adaptations to hematophagy and parasite infection. *Proc Natl Acad Sci U S A.* 112(48):14936–14941.
- Mieczkowski PA, Lemoine FJ, Petes TD. 2006. Recombination between retrotransposons as a source of chromosome rearrangements in the yeast *Saccharomyces cerevisiae*. *DNA Repair (Amst).* 5(9–10):1010–1020.
- Monti V, Lombardo G, Loxdale HD, Manicardi GC, Mandrioli M. 2012. Continuous occurrence of intra-individual chromosome rearrangements in the peach potato aphid, *Myzus persicae* (Sulzer) (Hemiptera: Aphididae). *Genetica* 140(1–3):93–103.
- Moran NA. 1992. The evolution of aphid life cycles. *Annu Rev Entomol.* 37(1):321–348.
- Nicholson SJ, Nickerson ML, Dean M, Song Y, Hoyt PR, Rhee H, Kim C, Puterka GJ. 2015. The genome of *Diuraphis noxia*, a global aphid pest of small grains. *BMC Genomics.* 16(1):429.
- Nouhaud P, Gautier M, Gouin A, Jaquiéry J, Peccoud J, Legeai F, Mieuze L, Sradja CM, Lemaître C, Vitalis R, et al. 2018. Identifying genomic hotspots of differentiation and candidate genes involved in the adaptive divergence of pea aphid host races. *Mol Ecol.* 27(16):3287–3300.
- Nowell RW, Almeida P, Wilson CG, Smith TP, Fontaneto D, Crisp A, Micklem G, Tunnacliffe A, Boschetti C, Barraclough TG. 2018. Comparative genomics of bdelloid rotifers: insights from desiccating and nondesiccating species. *PLoS Biol.* 16(4):e2004830.
- Pal A, Vicoso B. 2015. The X chromosome of hemipteran insects: conservation, dosage compensation and sex-biased expression. *Genome Biol Evol.* 7(12):3259–3268.
- Panfilio KA, Vargas Jentszsch IM, Benoit JB, Erezylmaz D, Suzuki Y, Colella S, Robertson HM, Poelchau MF, Waterhouse RM, Ioannidis P, et al. 2019. Molecular evolutionary trends and feeding ecology diversification in the Hemiptera, anchored by the milkweed bug genome. *Genome Biol.* 20(1):1–26.
- Panigrahi CB, Patnaik SC. 1991. Intraspecific chromosomal variation in five species of aphids (Aphididae: Homoptera: Insecta). *Cytologia (Tokyo)* 56(3):379–387.
- Panzera F, Pérez R, Hornos S, Panzera Y, Cestau R, Delgado V, Nicolini P. 1996. Chromosome numbers in the Triatominae (Hemiptera–Reduviidae): a review. *Mem Inst Oswaldo Cruz.* 91(4):515–518.
- Peccoud J, Ollivier A, Plantegenest M, Simon J-C. 2009. A continuum of genetic divergence from sympatric host races to species in the pea aphid complex. *Proc Natl Acad Sci U S A.* 106(18):7495–7500.
- Peccoud J, Simon J. 2010. The pea aphid complex as a model of ecological speciation. *Ecol. Entomol.* 35:119–130.
- Piazza A, Heyer WD. 2019. Homologous recombination and the formation of complex genomic rearrangements. *Trends Cell Biol.* 29(2):135–149.
- Pimentel H, Bray NL, Puente S, Melsted P, Pachter L. 2017. Differential analysis of RNA-seq incorporating quantification uncertainty. *Nat Methods.* 14(7):687–690.
- Price MN, Dehal PS, Arkin AP. 2009. FastTree: computing large minimum evolution trees with profiles instead of a distance matrix. *Mol Biol Evol.* 26(7):1641–1650.
- Price MN, Dehal PS, Arkin AP. 2010. FastTree 2—approximately maximum-likelihood trees for large alignments. *PLoS One* 5(3):e9490.
- Purandare SR, Bickel RD, Jaquiery J, Rispe C, Brisson JA. 2014. Accelerated evolution of morph-biased genes in pea aphids. *Mol Biol Evol.* 31(8):2073–2083.
- Quinlan AR, Hall IM. 2010. BEDTools: a flexible suite of utilities for comparing genomic features. *Bioinformatics* 26(6):841–842.
- Richard G, Legeai F, Prunier-Leterme N, Bretaudeau A, Tagu D, Jaquiéry J, Le Trionnaire G. 2017. Dosage compensation and sex-specific epigenetic landscape of the X chromosome in the pea aphid. *Epigenet Chromatin.* 10:30.
- Rieseberg LH. 2001. Chromosomal rearrangements and speciation. *Trends Ecol Evol.* 16(7):351–358.
- Ris H. 1942. A cytological and experimental analysis of the meiotic behavior of the univalent X chromosome in the bearberry aphid *Tamalia (=Phyllaphis) coweni* (Ckll.). *J Exp Zool.* 90(2):267–330.
- Ris H. 1943. A quantitative study of anaphase movement in the aphid *Tamalia*. *Biol Bull.* 85(2):164–178.
- Roach MJ, Schmidt SA, Borneman AR. 2018. Purge Haplotigs: allelic contig reassignment for third-gen diploid genome assemblies. *BMC Bioinf.* 19(1):460.
- Ruan J, Li H. 2019. Fast and accurate long-read assembly with wtdbg2. *Nat Methods.* 17(2):155–158.
- Schaeffer SW. 2018. Muller “elements” in *Drosophila*: how the search for the genetic basis for speciation led to the birth of comparative genomics. *Genetics* 210(1):3–13.
- Schalamun M, Nagar R, Kainer D, Beavan E, Eccles D, Rathjen JP, Lanfear R, Schwessinger B. 2019. Harnessing the MinION: an example of how to establish long-read sequencing in a laboratory using challenging plant tissue from *Eucalyptus pauciflora*. *Mol Ecol Resour.* 19(1):77–89.
- Schild DR, Card DC, Hales NR, Pery BW, Pasquesi GM, Blackmon H, Adams RH, Corbin AB, Smith CF, Ramesh B, et al. 2019. The origins and evolution of chromosomes, dosage compensation, and mechanisms underlying venom regulation in snakes. *Genome Res.* 29(4):590–601.
- Schrader F. 1947. The role of the kinetochore in the chromosomal evolution of the Heteroptera and Homoptera. *Evolution (N Y).* 1(3):134–142.
- Sharp AJ, Spetswood HT, Robinson DO, Turner BM, Jacobs PA. 2002. Molecular and cytogenetic analysis of the spreading of X inactivation in X; autosome translocations. *Hum Mol Genet.* 11(25):3145–3156.
- Shen W, Le S, Li Y, Hu F. 2016. SeqKit: a cross-platform and ultrafast toolkit for FASTA/Q file manipulation. *PLoS One* 11(10):e0163962.
- Simão FA, Waterhouse RM, Ioannidis P, Kriventseva EV, Zdobnov EM. 2015. BUSCO: assessing genome assembly and annotation completeness with single-copy orthologs. *Bioinformatics* 31(19):3210–3212.
- Simon J-C, Rispe C, Sunnucks P. 2002. Ecology and evolution of sex in aphids. *Trends Ecol. Evol.* 17(1):34–39.
- Smit AFA, Hubley R. 2008. RepeatModeler Open-1.0. Available from: <https://www.repeatmasker.org>.
- Smit AFA, Hubley R, Green P. 2005. RepeatMasker Open-4.0.
- Smit AFA, Hubley R, Green P. 2015. RepeatMasker Open-4.0. 2013–2015.
- Startek M, Szafranski P, Gambin T, Campbell IM, Hixson P, Shaw CA, Stankiewicz P, Gambin A. 2015. Genome-wide analyses of LINE-LINE-mediated nonallelic homologous recombination. *Nucleic Acids Res.* 43(4):2188–2198.
- Stewart NB, Rogers RL. 2019. Chromosomal rearrangements as a source of new gene formation in *Drosophila yakuba*. *PLoS Genet.* 15(9):e1008314.
- Sved JA, Chen Y, Shearman D, Frommer M, Gilchrist AS, Sherwin WB. 2016. Extraordinary conservation of entire chromosomes in insects over long evolutionary periods. *Evolution (N Y).* 70(1):229–234.
- Tandonnet S, Koutsououlos GD, Adams S, Cloarec D, Parihar M, Blaxter ML, Pires-daSilva A. 2019. Chromosome-wide evolution and sex determination in the three-sexed nematode *Auanema rhodensis*. *G3 (Bethesda)*. 9:1211–1230.
- Tarailo-Graovac M, Chen N. 2009. Using RepeatMasker to identify repetitive elements in genomic sequences. *Curr Protoc Bioinf.* Chapter 4:Unit 4.10.
- Teterina AA, Willis JH, Phillips PC. 2020. Chromosome-level assembly of the *Caenorhabditis remanei* genome reveals conserved patterns of nematode genome organization. *Genetics* 214(4):769–780.
- Thorpe P, Escudero-Martinez CM, Cock PJAA, Eves-Van Den Akker S, Bos JBB. 2018. Shared transcriptional control and disparate gain and loss of aphid parasitism genes. *Genome Biol Evol.* 10(10):2716–2733.

- Ueshima N. 1966. Cytotaxonomy of the triatominae (Reduviidae: Hemiptera). *Chromosoma* 18(1):97–122.
- Vaser R, Sović I, Nagarajan N, Šikić M. 2017. Fast and accurate de novo genome assembly from long uncorrected reads. *Genome Res.* 27(5):737–746.
- Walker BJ, Abeel T, Shea T, Priest M, Abouelliel A, Sakthikumar S, Cuomo CA, Zeng Q, Wortman J, Young SK, et al. 2014. Pilon: an integrated tool for comprehensive microbial variant detection and genome assembly improvement. *PLoS One* 9(11):e112963.
- Wang L, Tang N, Gao X, Chang Z, Zhang L, Zhou G, Guo D, Zeng Z, Li W, Akinyemi IA, et al. 2017. Genome sequence of a rice pest, the white-backed planthopper (*Sogatella furcifera*). *Gigascience* 6(1):1–9.
- Wang Y, Tang H, DeBarry JD, Tan X, Li J, Wang X, Lee T-H, Jin H, Marler B, Guo H, et al. 2012. MCLScanX: a toolkit for detection and evolutionary analysis of gene synteny and collinearity. *Nucleic Acids Res.* 40(7):e49.
- Waterhouse RM, Seppey M, Simão FA, Manni M, Ioannidis P, Klioutchnikov G, Kriventseva EV, Zdobnov EM. 2018. BUSCO applications from quality assessments to gene prediction and phylogenomics. *Mol Biol Evol.* 35(3):543–548.
- Weisenfeld NI, Kumar V, Shah P, Church DM, Jaffe DB. 2017. Direct determination of diploid genome sequences. *Genome Res.* 27(5):757–767.
- Wellband K, Mérot C, Linnansaari T, Elliott JAK, Curry RA, Bernatchez L. 2019. Chromosomal fusion and life history-associated genomic variation contribute to within-river local adaptation of Atlantic salmon. *Mol Ecol.* 28(6):1439–1459.
- Wenger JA, Cassone BJ, Legeai F, Johnston JS, Bansal R, et al. 2020. Whole genome sequence of the soybean aphid, *Aphis glycines*. *Insect Biochem Mol Biol.* 123:102917.
- Wilson A, Sunnucks P, Hales D. 1997. Random loss of X chromosome at male determination in an aphid, *Sitobion* near *fragariae*, detected using an X-linked polymorphic microsatellite marker. *Genet Res.* 69(3):233–236.
- Xue J, Zhou X, Zhang C-X, Yu L-L, Fan H-W, Wang Z, Xu H-J, Xi Y, Zhu Z-R, Zhou W-W, et al. 2014. Genomes of the rice pest brown planthopper and its endosymbionts reveal complex complementary contributions for host adaptation. *Genome Biol.* 15(12):521.
- Yandell M, Ence D. 2012. A beginner's guide to eukaryotic genome annotation. *Nat Rev Genet.* 13(5):329–342.
- Yeo S, Coombe L, Warren RL, Chu J, Birol I. 2018. ARCS: scaffolding genome drafts with linked reads. *Bioinformatics* 34(5):725–731.
- Yi L, Pimentel H, Bray NL, Pachter L. 2018. Gene-level differential analysis at transcript-level resolution. *Genome Biol.* 19(1):11.
- Zheng GXY, Lau BT, Schnall-Levin M, Jarosz M, Bell JM, Hindson CM, Kyriazopoulou-Panagiotopoulou S, Masquelier DA, Merrill L, Terry JM, et al. 2016. Haplotyping germline and cancer genomes with high-throughput linked-read sequencing. *Nat Biotechnol.* 34(3):303–311.